In vivo analysis revealed that the significant antitumor effect of Ad-NK4 was mediated in part by inhibition of angiogenesis and that the antitumor effect of GEM was limited to its antiproliferative influence. GEM had no influence on angiogenesis. Thus, the high rate of apoptosis in combination therapy was induced by the complementary actions of the two treatments, namely antiproliferation by GEM and antiangiogenesis by NK4. *In vitro*, Ad-NK4 infection potently inhibited invasion of cancer cells in response to HGF and had no effect on proliferation. GEM exerted a very limited effect on invasive ability but showed a powerful antiproliferative effect similar to that observed in the *in vivo* study. Therefore, the strong *in vivo* antitumor effect of combination therapy with Ad-NK4 plus GEM was due to inhibition of proliferation, motility, and angiogenesis.

In our *in vivo* studies, treatment with Ad-NK4, which showed no antiproliferative effect, prevented tumor angiogenesis and subsequently increased apoptosis and prolonged survival. Strong antiangiogenic activity of NK4 in pancreatic cancer has been reported previously in our various *in vivo* studies of subcutaneous and orthotopic transplantation, peritoneal dissemination, and liver metastasis.[8,24–26] Saimura *et al*.[27] reported that an NK4 cDNA-transfected pancreatic cancer clone showed significant growth inhibition and reduced tumor vessel growth *in vivo*, although this clone showed an insufficient expression of NK4 to antagonize HGF. Therefore, at least in that study, the significant antitumor effect of NK4 *in vivo* depended mainly on its function as an angiogenesis inhibitor rather than as an HGF antagonist. NK4 inhibits growth and migration of microvascular endothelial cells stimulated by VEGF or bFGF as well as by HGF *in vitro*,[19] indicating that the antiangiogenic activity of NK4 is independent of its activity as an HGF antagonist. Putative binding molecules for NK4 may exist on endothelial cells, or unknown intracellular signals may interrupt VEGF/bFGF-mediated angiogenesis after inhibition of c-Met phosphorylation by NK4.

Significant inhibition of tumor growth in response to combination therapy was clear compared to the antitumor effect of high-dose GEM. A high dose of GEM, 320 mg/kg, increased tumor suppression by only 7% compared to that with 80 mg/kg of GEM (from 75 to 82%). Combination treatment of Ad-NK4 plus 80 mg/kg GEM compared to treatment with GEM alone suppressed tumor growth by 16% (from 75 to 91%) without increased toxicity. These results clearly indicate the efficient antitumor effect of combination therapy in the control of local growth of implanted tumors.

An antimetastatic effect of combination therapy may have led to prolonged survival. The most devastating aspect of pancreatic cancer is its early systemic dissemination and distant metastases; most deaths are related to metastasis. We have documented that antiangiogenic activity is important in the suppression of peritoneal dissemination.[8,25,27] Metastasis comprises stepwise cell attachment, angiogenesis, proliferation, and invasion, and it is important to regulate these steps.[28] NK4 interferes with invasion of cancer cells and tumor angiogenesis by means of its bifunctional properties as an HGF antagonist and an angiogenesis inhibitor.[19,29] GEM inhibits proliferation of metastasized cells. Therefore, combination therapy inhibits three steps of tumor metastasis: angiogenesis, proliferation, and invasion. As a result, combination therapy completely suppressed both peritoneal dissemination and liver metastasis, resulting in prolonged survival.

Clinical trials of GEM combined with several antitumor agents have been conducted for pancreatic cancer.[30] However, the majority of these therapies used cytotoxic drugs, such as docetaxel, 5FU, cisplatin, and irinotecan.[31–35] Although these cytotoxic drugs exert antitumor effects by different mechanisms, the applicable dose of each drug is limited due to cumulative systemic toxicity. In such clinical trials, combination therapy may result in more adverse effects despite the expected additive antitumor effects. Because of the lack of an antiproliferative effect of NK4 on normal cells as well as cancer cells, the toxicity of combination therapy of Ad-NK4 plus GEM should be minimized. In fact, as shown in the present study, combination of sufficient doses of a cytotoxic agent, GEM, plus Ad-NK4 provided maximum antitumor effects without escalating toxicity.

Cancer gene therapy is generally at a stage of proof of principles and safety. In considering clinical trials of Ad-NK4 for pancreatic cancer, it is important to inject Ad-NK4 into the tumor mass instead of delivering it systemically because a large amount of NK4 protein delivered to the tumor is necessary for complete inhibition of HGF activity and for significant suppression of tumor growth. Clinical trials of gene therapy plus GEM treatment have been reported, for example, with conditionally replicating adenovirus (ONYX-015) or adenovirus encoding interleukin-12 injected into the tumor under endoscopic ultrasonographic (EUS) control.[36,37] In these studies, severe complications, including pancreatitis, did not occur. Peritumoral injection of Ad-NK4 under EUS control in combination with GEM would be safe and effective for patients with advanced pancreatic cancer.

In summary, we showed that peritumoral injection of Ad-NK4 combined with weekly GEM treatment significantly reduced growth and metastasis of human pancreatic cancer cells implanted orthotopically into nude mice and prolonged survival of the mice. Inhibition of primary tumor growth, liver metastasis, and peritoneal dissemination was mediated by the bifunctional effects of NK4 as an HGF antagonist and an angiogenesis inhibitor and by the direct antitumor effect of GEM. Clinical trials to assess the safety and validity of Ad-NK4 in combination with GEM are warranted in patients with pancreatic cancer.

References

1 FFCR. *Cancer Statistics in Japan* 2003.
2 Niederhuber JE, Brennan MF, Menck HR. The National Cancer Data Base report on pancreatic cancer. *Cancer* 1995; 76: 1671–1677.

Rapid and Sensitive Assay of *K-ras* Mutations in Pancreatic Cancer by Electrochemical Detection with Ferrocenyl-naphthalene-diimide

NAMI ISHIKAWA[1], TAKAHITO MIYA[2], KAZUHIRO MIZUMOTO[1], KENOKI OHUCHIDA[1], EISHI NAGAI[1], KOJI YAMAGUCHI[1], MASAHIKO AMANO[2], SHIGEORI TAKENAKA[3] and MASAO TANAKA[1]

[1]*Department of Surgery and Oncology, Graduate School of Medical Sciences, Kyushu University, 3-1-1 Maidashi, Higashi-ku, Fukuoka 812-8582;*
[2]*TUM gene, Inc., 3-1 Kazusa-Koito Kimitsu, Chiba 292-1149;*
[3]*Department of Material Science, Kyushu Institute of Technology, 1-1, Sensui-cho, Tobata-ku, Kitakyushu, Fukuoka 804-8550, Japan*

Abstract. *The DNA chip is a very powerful tool for genetic analysis. Conventional DNA chips that utilize fluorescence detection systems are very complicated, expensive and impractical, but the electrochemical array (ECA) chip is gaining popularity. To investigate the validity of the ECA chip, which utilizes ferrocenyl-naphthalene-diimide (FND), k-ras mutations in 20 pancreatic cancer tissues were examined. DNA was isolated from 20 pancreatic cancer tissues and subjected to a 2-stage polymerase chain reaction (PCR). The k-ras mutations were detected with the ECA chip. To verify the reliability of the ECA chip, the DNA was also analyzed by direct sequencing and the PCR-dependent preferential homoduplex formation assay (PCR-PHFA). The ECA chip could detect one mutation in a background of 1000 wild-type DNAs. K-ras mutations were identified in 17 out of 20 (85%) pancreatic cancer samples. Three mutations of codon 12 of k-ras, GTT, GAT and AGT, were detected. K-ras mutations were detected in 13 out of 20 (65%) samples by sequencing and in 17 out of 20 (85%) samples by PCR-PHFA. These findings were concordant with the ECA chip result. The FND-ECA chip is a sensitive, rapid and reliable method for screening point mutations in a variety of clinical samples.*

Correspondence to: Kazuhiro Mizumoto, Department of Surgery and Oncology, Graduate School of Medical Sciences, Kyushu University, 3-1-1 Maidashi, Higashi-ku, Fukuoka 812-8582, Japan. Tel: +81-92-642-5441, Fax: +81-92-642-5458, e-mail: mizumoto@surg1.med.kyushu-u.ac.jp

Key Words: Electrochemical array (ECA) chip, ferrocenyl-naphthalene-diimide (FND), *k-ras* mutation, restriction enzyme *BstN*I, assymmetric PCR (A-PCR).

DNA chips have been in use since the late 1980s and this technology has been a very powerful and valuable tool for genetic analysis because it is sensitive, specific, accurate, quick and versatile. Fluorescence labeling is typically used to visualize hybridization on chips (1). Despite the high accuracy and sensitivity of fluorescence detection systems, fluorescence readers are expensive and difficult to handle. Therefore, DNA chips cannot be commonly used as a routine diagnostic tool at present.

Electrochemical detection systems have gained popularity since the early 1990s, and several electrochemical DNA sensors that transduce DNA information into electrochemical signals have been developed (2-4). The detection of mutations by most of these sensors is based on the difference in thermal stability between mismatched and fully matched DNA duplexes. However, assessments of thermal stability require precise temperature control, which is expensive and difficult to accomplish, as well as significant amounts of time. We developed ferrocenyl-naphthalene-diimide (FND) as a hybridization indicator specific for double-stranded DNA (5, 6). FND intercalates into double-stranded DNA but cannot interact with single-stranded DNA (7, 8). When target DNA hybridizes to a probe immobilized on the electrodes of the ECA chip, the FND concentrated on the electrodes gives rise to an electrochemical signal proportional to the amount of hybridized target DNA (9, 10).

Pancreatic cancer is the fourth leading cause of cancer-related death in the world (11). Because pancreatic cancers tend to grow rapidly, invade adjacent organs and metastasize, they are difficult to diagnose and treat at an early stage. Many techniques for detecting tumors of the pancreas at an early stage have been developed and improved over the past decades; however, the results to date have not been

Table IA. *Primer design.*

PCR	Primer name	Primer sequence	Expected product size (bp)	Specific notes
For the first PCR				
First diagnostic	Kras12MvaI 1213SeqR	GAATATAAACTTGTGGTAGTTGGAcCT CTGTATCAAAGAATGGTCCTGC	159	Amplify a fragment of *k-ras* exon 1. Presence of amplicon indicates that the template has mutant *k-ras*.
First control	PCRcontF2 PCRcontR	GGTGTAGTGGAAACTAGGAATTAC CTTACCTGTCTTGTCTTTGCTG	291	Control of PCR
First *BstN*I control	MvaIcontF3 MvaIcontR4	AATTACTCTTACCAATGCAACAGAC CTACACCTAAGTAGTTCTAAAGTGG	279	Amplify a fragment of *k-ras* exon 4a that contains *BstN*I site. Presence of amplicon indicates *BstN*I failure.
For the second PCR				
A-PCR diagnostic	Kras12MvaI 1213R2	GAATATAAACTTGTGGTAGTTGGAcCT TTGTTGGATCATATTCGTCCAC	100	Amplify a fragment of *k-ras* exon 1. Presence of amplicon indicates that the template has mutant *k-ras*.
A-PCR control	PCRcontF PCRcontR2	TTATGACAAAAGTTGTGGACAGG CTTCTTGCTAAGTCCTGAGCC	197	Control for PCR
A-PCR *BstN*I control	MvaIcontF4 MvaIcontR2	GCTTTTTATACATTGGTGAGGGAG TGGTTGCCACCTTGTTACC	183	Amplify a fragment of *k-ras* exon 4a that contains *BstN*I site. Presence of amplicon indicates *BstN*I failure.
Special diagnostic	Kras12-1LP	P-GTGGCGTAGGCAATGATTCTGAA TTAGCTGTATCGTCAAGGCACTC	204	Amplify the single-strand target for variant of the first letter at *k-ras* codon 12 of exon 1.
	Kras12-2LP	P-TGGCGTAGGCAAGTGATCTGAAT TAGCTGTATCGTCAAGGCACTC	204	Amplify the single-strand target for variant of the second letter at *k-ras* codon 12 of exon 1.
Special control	PCRcontLP	P-TGTTACTAATGACTGTGTTTGTCTCT GGGAAAGAAAAAAAAGTTATAGCAC	151	Control for PCR
Special *BstN*I control	MvaIcontLP	P-CAAAGAAGAAAAGACTCTGCATTTT TTAATTTTCACACAGCCAGGAG	114	Amplify a single-stranded fragment of *k-ras* exon 4a that contain s *BstN*I site. Presence of amplicon indicates *BstN*I failure.

Table IB. *Probe design.*

Probe	Target	Probe sequence
Control PCR (PC)		HS-TATGACAAAAGTTGTGGACAGGTTTTGAAAGATATTTG
Control *BstN*I (RC)		HS-GTGAGGGAGATCCGACAATACAGATTGAAAAAAATCAG
Mutant probe (1C)	CGT	HS-GAAAATGACTGAATATAAACTTGTGGTAGTTGGAcCac
Mutant probe (1A)	AGT	HS-GAAAATGACTGAATATAAACTTGTGGTAGTTGGAcCaa
Mutant probe (1T)	TGT	HS-GAAAATGACTGAATATAAACTTGTGGTAGTTGGAcCat
Mutant probe (2C)	GCT	HS-AAAATGACTGAATATAAACTTGTGGTAGTTGGAcCgGc
Mutant probe (2A)	GAT	HS-AAAATGACTGAATATAAACTTGTGGTAGTTGGAcCIIa
Mutant probe (2T)	GTT	HS-AAAATGACTGAATATAAACTTGTGGTAGTTGGAcCgGt

satisfactory. Therefore, it is necessary to develop more effective systems to screen for pancreatic cancer (12, 13).

The mutation of codon 12 of exon 1 of *k-ras* is one of the most common alterations in pancreatic cancer with a frequency of 75-90% (14). *K-ras* mutations in various cancers have been analyzed, however, *k-ras* mutations in pancreatic cancers have never been analyzed with an FND-ECA chip. The aim of the present study was to investigate the validity and practicality of the FND-ECA chip as a diagnostic test tool, by examining *k-ras* mutations in pancreatic cancer cell lines and tissues and comparing the results with those of conventional techniques.

Materials and Methods

Tumor cell lines. Four pancreatic cancer cell lines, A549, MIA Paca2, LS174T and SW480, each containing a mutation in codon 12 of *k-ras*, were used. The GGT sequence of codon 12 is mutated to AGT in A549 cells, TGT in MIA Paca2 cells, GAT in LS174T cells and

GTT in SW480 cells. The human umbilical vein endothelial cell line (HuVEC), which has no *k-ras* mutations, was used as the control. The HuVEC cell line was purchased from Kurabo (Tokyo, Japan), A549 and MIAPaca2 were obtained from the Japanese Cancer Resource Bank (Tokyo, Japan), LS174T was obtained from the European Collection of Animal Cell Culture (Wiltshire, UK) and SW480 was purchased from the American Type Culture Collection (Rockville, MD, USA).

Tissue samples. Pancreatic cancer tissues were obtained from 20 patients who were diagnosed and treated by surgical resection during the period April 2000 to March 2003 at the Department of Surgery and Oncology, Graduate School of Medical Science, Kyushu University (Fukuoka, Japan). The study was conducted according to the recommendations of the World Medical Association Declaration of Helsinki. Informed consent was obtained from all patients and the study was approved by the Institutional Review Board of Kyushu University. The pancreatic tissues were frozen at –80°C immediately after resection.

DNA extraction. Genomic DNA was extracted by means of a standard phenol and chloroform method (15) from the cell lines and pancreatic cancer tissues. The tissue specimens were digested in sodium dodecylsulfate (SDS) and proteinase K at 56°C overnight and genomic DNA was extracted with phenol-chloroform and precipitated with ethanol.

Primer and probe design. The sequences of primers and probes used for this experiment are shown in Table I. All oligonucleotides used in this research were custom-synthesized by Operon Biotechnologies K.K. (Tokyo, Japan).

Polymerase chain reaction (PCR). Two-stage PCR reactions are needed to detect single nucleotide mutations with FND-ECA chips. In the first PCR, a 159-bp region of *k-ras* codon 12 of exon 1 is amplified from genomic DNA in the presence of the restriction enzyme *BstN*I, while in the second PCR, a specific single-stranded target DNA is made from the product of the first PCR. The second PCR is an asymmetric PCR (A-PCR).

For the first PCR, 3 sets of primers were used (Table IA). The diagnostic primers Kras-12 MvaI and 1213 SeqR were used to amplify a 159-bp fragment of exon 1 of the *k-ras* gene that contains a *BstN*I site (CCTGG) in wild-type *k-ras* amplicons. Because *BstN*I is included in the first PCR, wild-type *k-ras* cannot be amplified, whereas the mutant DNA that lacks the *BstN*I cleavage site is selectively amplified by these primers. The PCR control primers PCRcontF2 and PCRcontR amplify a 291-bp fragment of exon 4a of *k-ras* as a control for the PCR conditions. Restriction enzyme control primers MvalcontF3 and MvalcontR4 amplify a 279-bp fragment of exon 3 that contains a *BstN*I cleavage site. The presence of this amplicon indicates that *BstN*I digestion failed. For the PCR, 50 ng of genomic DNA template were added to a 20-µl reaction solution containing 0.1 µM of each diagnostic primer (Kras-12 MvaI and 1213 SeqR), 0.05 µM of each PCR control primer (PCRcontF2 and PCRcontR), 0.1 µM of each enzyme control primer (MvalcontF3 and MvalcontR4), 10 U *BstN*I, 1 U Taq polymerase-Hot Start version (Takara Bio, Shiga, Japan), 2 mM dNTP and 10 x PCR buffer. After predenaturation at 94°C for 2 min, 15 cycles of PCR amplification (denaturation at 94°C for 30 sec, annealing at 60°C for 60 sec and elongation at 72°C for 10 sec), were performed followed by a final elongation at 72°C for 30 sec. The products were analyzed by electrophoresis on 10% acrylamide gels.

In the second PCR (A-PCR), 2 µl of PCR product were added to 20 µl of the second PCR solution that contained 1 µM special diagnostic primer (Kras12-1LP or Kras12-2LP, Table IA), which amplify the single-strand target DNAs, with mutations of the first or second position of codon 12, 0.25 µM special PCR control primer (PCRcontLP, Table IA), 1 µM *BstN*I control primer (MvalcontLP, Table IA), 0.1 µM of each diagnostic primer (Kras-12 MvaI and 1213R2, Table IA), 0.05 µM of each PCR control primer (PCRcontF and PCRcontR2, Table IA), 0.1 µM of each enzyme control primer (MvalcontF4 and MvalcontR2, Table IA), 1 U Taq polymerase-Hot Start version, 0.25 mM dNTP and 10x PCR buffer. Two primer sets, set 1 and set 2, which contained Kras12-1LP and Kras12-2LP, respectively, were prepared to amplify 3 SNP targets with one set simultaneously. Set 1 and set 2 corresponded to variants of the first and second letter at *k-ras* codon 12, respectively. To amplify single-strand-specific targets that were hybridized to probes on the ECA chip, only the special primer was applied, making the second PCR an asymmetric PCR (A-PCR). The A-PCR consisted of an initial activation of polymerase at 94°C for 2 min, followed by 40 cycles of PCR amplification (denaturation at 94°C for 30 sec, annealing at 60°C for 60 sec and elongation at 72°C for 10 sec), and final elongation at 72°C for 30 sec and denaturation at 95°C for 1 min. After confirmation of the quality of the PCR products by electrophoresis on a 10% acrylamide gel, the A-PCR products were subjected to hybridization and electrochemical measurement with the ECA chip.

Preparation of ECA chip-immobilized DNA probe. Mutant probes for 6 *k-ras* gene mutations and 2 control probes (M probes and C probes listed in Table IB) were immobilized on individual gold electrodes of an ECA chip, as described previously (6).

Hybridization, ligation and electrochemical measurement. Prior to hybridization of the A-PCR products to the C or M probes immobilized on the gold electrodes of an ECA chip, the ECA chip was denatured and the baseline current (I_0) was measured, as described previously (16). The A-PCR products (10 µl) were hybridized to the probes at room temperature for 10 min. The ligation reaction between the A-PCR products and the probes was then carried out at room temperature for 5 min. The ECA chip was subsequently denatured, washed and used for the electrochemical measurement. Measurement of electric current (I_1) was performed at room temperature with an electrochemical analyzer, STR3000 (TUM Gene, Inc. Kimitsu, Japan). The results were evaluated by the score calculated from the following equation. ΔI is the hybridization/ligation efficiency of a probe and is calculated as $\Delta I=(I_1 - I_0)/ I_0 \times 100$. The procedure from hybridization to electrochemical measurement (I_0, I_1) takes less than 1 h.

Direct DNA sequencing analysis and PCR-preferential homoduplex formation assay (PCR-PHFA). To verify the reliability of the ECA chip data, DNAs extracted from all samples were analyzed by direct DNA sequencing and PCR-PHFA. Direct sequencing was done with the dideoxy chain termination method with a BigDye Terminator V1.1 Cycle Sequencing Kit (PE Applied Biosystems) and an automated DNA sequencer (ABI PRISM 3100, PE Applied Biosystems). PCR-PHFA was carried out with a commercially available kit (Wakunaga Pharmaceutical, Hiroshima, Japan).

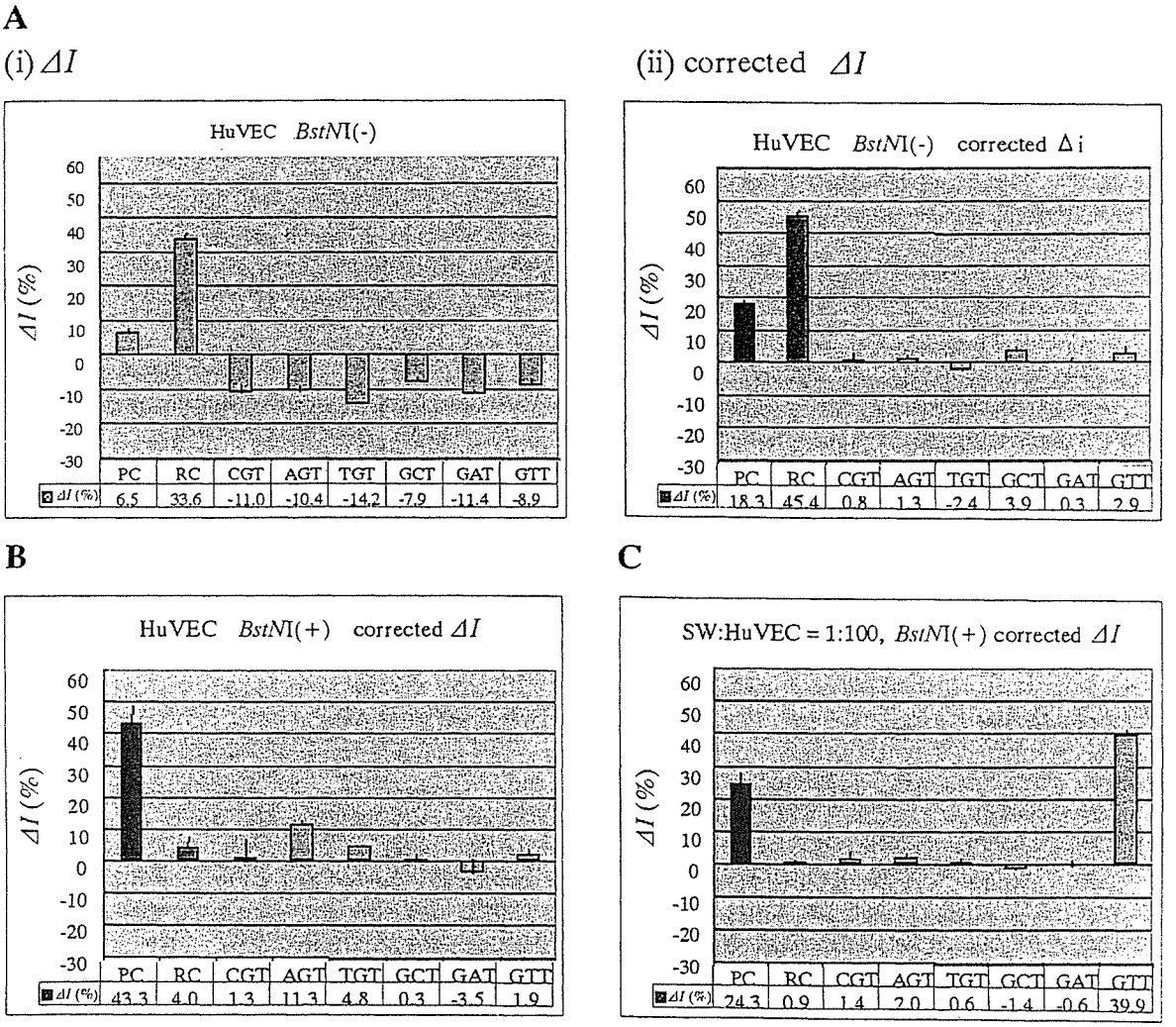

Figure 1. *ECA chip analysis of cell lines. A. HuVECs (wild-type) amplified without restriction enzyme BstNI. (i)* $\Delta I = (I_1 - I_0)/I_0 \times 100$. *(ii) Corrected ΔI is the remainder after the average of the 4 lowest value data among 6 probes are substracted from each ΔI. B. HuVEC DNA amplified in reactions containing BstNI. C. SW480 cells carrying the GTT mutation in codon 12 of k-ras and 100-fold wild-type cells amplified in reactions containing BstNI.*

Results

Analysis of the ECA chip data. Two control probes and 6 mutant *k-ras* probes (Table IB) were immobilized on the ECA chip. One of the 2 control probes was the PCR C probe (PC) and the other the *BstN*I C probe (RC). The 6 mutant-specific probes were 1C/CGT, 1A/AGT, 1T/TGT, 2C/GCT, 2A/GAT, 2T/GTT and were designed to detect a mutational transition from GGT to CGT, AGT, TGT, GCT, GAT or GTT, respectively. The ECA chip analyses of the PCR products of the cell lines amplified with or without restriction enzyme are shown in Figure 1. In some cases, *ΔI* ($(I_1 - I_0)/I_0 \times 100$) yielded a negative value (Figure1A- (i)). When this happened, the average of the 4 lowest value data among the 6 probes was substracted from each *ΔI* and defined the value as a corrected *ΔI* (Figure 1A- (ii)). The collected *ΔI* was defined as positive when the value was more than 20%. When the first PCR was carried out without *BstN*I, the PCR product of wild-type DNA from HuVEC cells yielded a positive *ΔI* for both the PC and RC probes and a negative *ΔI* for the 6 mutant probes (Figure 1A- (ii)), indicating that the 2-stage PCR was carried out correctly and that the HuVEC DNA did not carry any *k-ras* mutations. When *BstN*I was included, the ECA chip yielded a positive *ΔI* for the PC probe. *ΔI* was negative for the RC probe, indicating that *BstN*I functioned appropriately in this system (Figure 1B). As shown in Figure 1C, the SW480 cells, which carry the GTT mutation of *k-ras* codon 12,

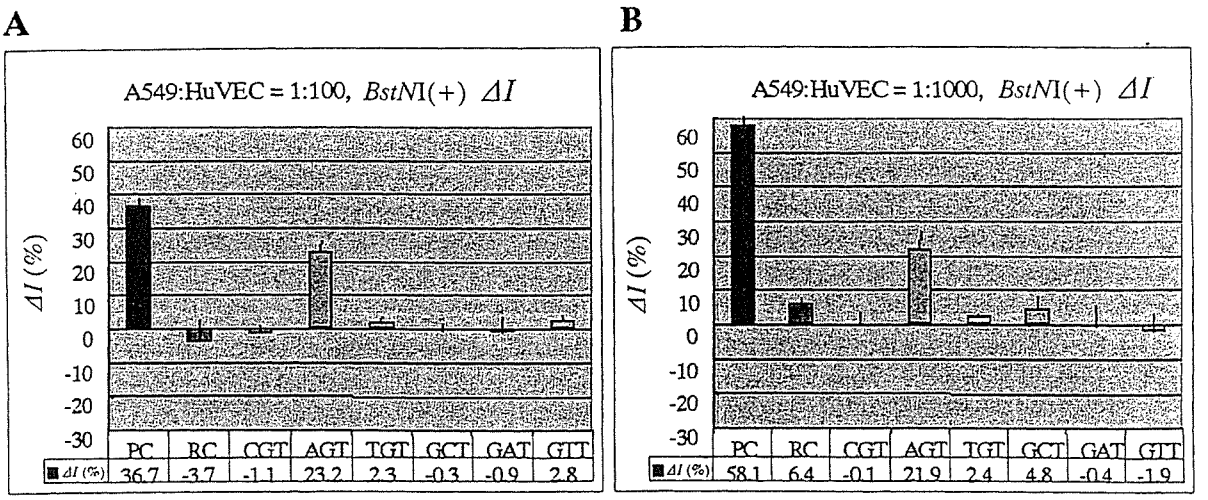

Figure 2. *Sensitivity of the ECA chip. The ECA chip detected the AGT mutation in codon 12 of k-ras in A549 cells mixed with 100-fold wild-type cells (A) and with 1000-fold wild-type cells (B).*

Table II. *Clinical data.*

Patient No.	Sex	Age (years)	Tumor site	TNM classification	Tumor stage[a]	Surgery	Outcome (months survival)
1	M	69	Phb	T4N1M0	IVa	TP+SP	Dead (9)
2	F	63	Pt	T3N1M0	III	DP+SP	Dead (17)
3	M	63	Ph	T4N1M0	IVa	PpPD	Dead (24)
4	F	69	Phb	T3N2M0	IVa	PD+IOR	Dead (9)
5	M	75	Ph	T3N1M0	III	PpPD	Dead (19)
6	M	36	Ph	T4N3M1	IVb	PD	Dead (7)
7	F	59	Ph	T4N1M0	IVa	PD	Dead (9)
8	M	75	Ph	T3N1M0	III	PD	n.d.
9	M	72	Pb	T3N0M0	III	DP+SP	Dead (34)
10	M	60	Pt	T4N1M0	IVa	TP+SP	Dead (5)
11	M	56	Ph	T3N1M0	III	PpPD	Dead (3)
12	M	62	Pb	T4N1M0	IVa	DP+SP	n.d.
13	M	58	Pb	T4N1M0	IVa	DP+SP	Alive (27)
14	F	57	Ph	T3N1M0	III	PpPD	Alive (32)
15	M	64	Ph	T3N0M0	III	PpPD	Alive (31)
16	F	61	Ph	T3N0M0	III	PpPD	Alive (30)
17	F	53	Ph	T4N3M1	IVb	PpPD	Dead (16)
18	M	72	Ph	T4N2M0	IVb	PpPD	Alive (28)
19	M	67	Pbt	T4N1M0	IVa	DP+SP	Dead (13)
20	F	64	Pbt	T3N1M0	III	DP+SP	Dead (5)

[a]Classification by Japan Pancreas Society.

showed a positive *ΔI* for the PC and GTT probes. The other 3 cell lines, A549 (GGT→AGT), MIA Paca2 (GGT→TGT) and LS174T (GGT→GAT), showed a positive *ΔI* for the PC probe and corresponding mutant probes (data not shown). These results showed that *k-ras* mutations can be identified accurately with the ECA chip.

Determination of the sensitivity of the ECA chip. To determine the sensitivity of the ECA chip, 4 tumor cell lines carrying *k-ras* mutations were mixed with 100- to 1000-fold wild-type HuVEC cells. When the A549 cell line was tested in a background of 100-fold wild-type HuVEC cells, more than 20% of *ΔI* was observed with the PC probe and mutant

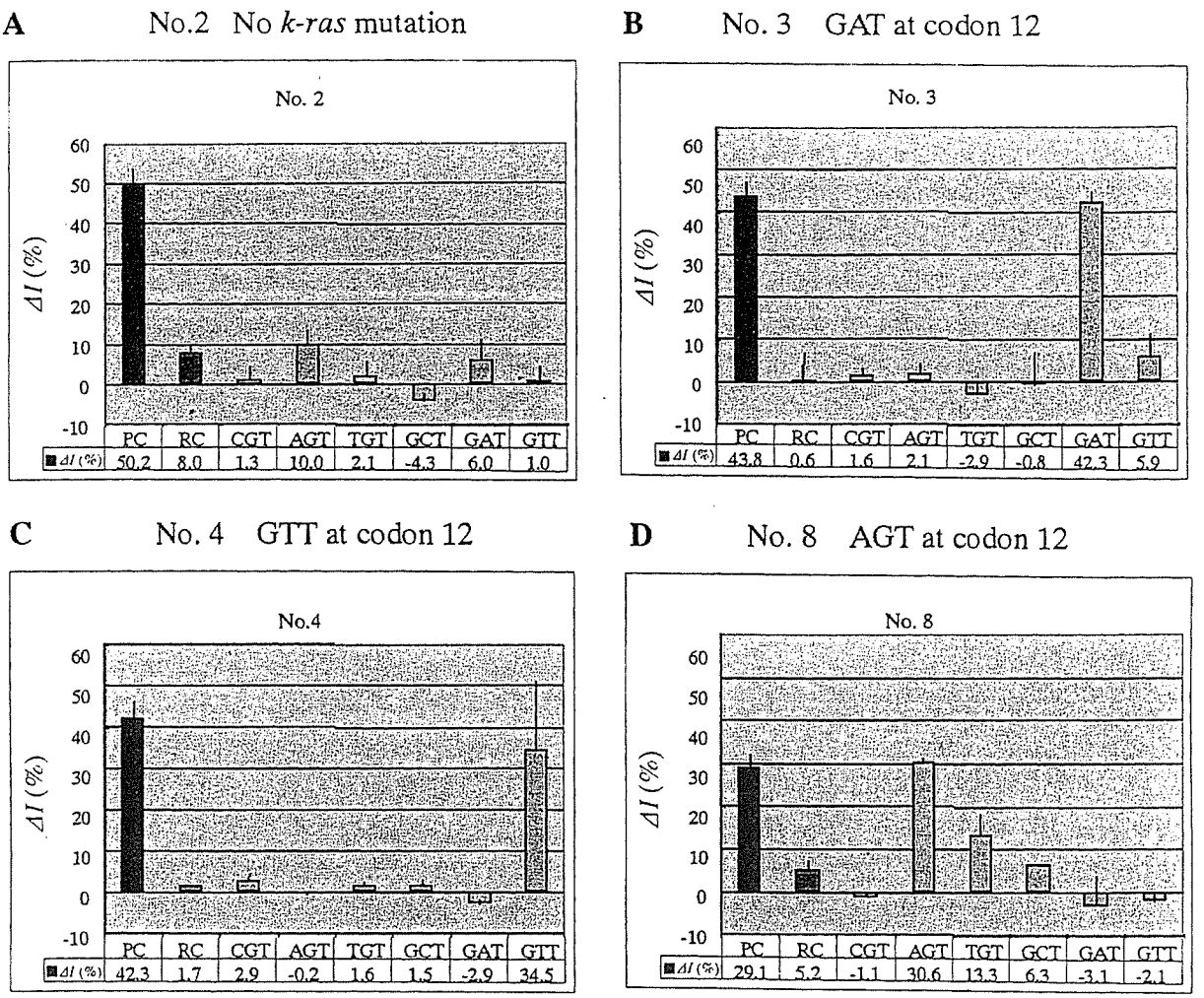

Figure 3. *ECA chip analysis of pancreatic cancer tissues. Three mutations in codon 12 of k-ras, GAT, GTT, and AGT were found on the 20 tissue samples investigated (B-D). ΔI over 20% was not obtained with any mutant probe in samples without k-ras mutations (A).*

probe for AGT (Figure 2A). A similar result was obtained when mutant DNA was mixed with 1000-fold excess wild-type DNA (Figure 2B). At a 10,000-fold excess of wild-type DNA, the mutation could not be detected (data not shown). In the other 3 cell lines, a positive *ΔI* was also detected for the mutant probe corresponding to each mutation and in the 1000-fold excess wild-type DNA (data not shown).

ECA chip analysis of tissue samples. DNAs extracted from 20 pancreatic cancer specimens were analyzed with the FND-ECA chip. The clinical features of the 20 pancreatic cancer patients are shown in Table II. Three mutations of codon 12 of *k-ras*, GAT, GTT and AGT, were identified (Figure 3) and mutations were present in DNAs from 17 out of 20 (85%) of the pancreatic cancer specimens. The GGT to GTT, GAT, or AGT mutations of codon 12 of *k-ras* were recognized in 12, 4, or 1 sample, respectively (Table III). Direct sequence analysis detected *k-ras* mutations (8 GTT, 4 GAT and 1 AGT) in 13 out of 20 samples (65%). PCR-PHFA identified mutations in 17 (85%) samples. These results were the same as the FND-ECA chip data, suggesting that the detection ability of the ECA chip data was superior to that of direct sequencing and similar to that of PCR-PHFA (Table IV).

Discussion

The present results indicate that the FND-ECA chip is a useful tool for the accurate, rapid and sensitive detection of *k-ras* mutations in human pancreatic cancer tissues. The mutation detection rate of the FND-ECA chip, 85%, was comparable to that of the highly sensitive PCR-PHFA

Table III. *K-ras mutations.*

	Direct sequence	ECA chip	PCR-PHFA
Total no. of positive cases	13	17	17
Type of *K-ras* mutation			
AGT	1	1	1
CGT	0	0	0
TGT	0	0	0
GAT	4	4	4
GCT	0	0	0
GTT	8	12	12

Table IV. *K-ras mutations in exon 1.*

Patient No.	Direct sequence	ECA chip	PCR-PHFA
1	(-)	GTT	GTT
2	(-)	(-)	(-)
3	GAT	GAT	GAT
4	GTT	GTT	GTT
5	GAT	GAT	GAT
6	GTT	GTT	GTT
7	GTT	GTT	GTT
8	AGT	AGT	AGT
9	GTT	GTT	GTT
10	GTT	GTT	GTT
11	GTT	GTT	GTT
12	(-)	GTT	GTT
13	(-)	(-)	(-)
14	GAT	GAT	GAT
15	GTT	GTT	GTT
16	(-)	GTT	GTT
17	GAT	GAT	GAT
18	(-)	GTT	GTT
19	(-)	(-)	(-)
20	GTT	GTT	GTT

method. Furthermore, the FND-ECA chip could detect different mutations and the measurement procedure takes less than 1 h. Pancreatic cancer tissues contain both cancer cells and non-cancerous cells, including normal duct, acinar, islet, inflammatory and fibroblast cells. Therefore, the FND-ECA chip must possess sufficient sensitivity to detect point mutations of tumor cells, at least, in a background of 100- to 1000-fold non-cancerous cells.

To increase the hybridization efficiency, 2-stage PCR was used. The first PCR containing *BstN*I allowed for the simultaneous amplification of mutant *k-ras* and the inhibition of the amplification of wild-type *k-ras*. The second PCR generated the single-stranded and self-looped target that allows high affinity binding to probes immobilized on the ECA chip. Ligation between a fixed probe and target increases the contrast between positive and negative signals. FND allows the ECA chip to detect double-stranded DNA efficiently (8). An FND-ECA chip can detect one mutant in a background of 1000 wild-type (Figure 2).

In the present study, the detection rate of mutations in codon 12 of *k-ras* was 85%, consistent with the frequency of 75-90% reported previously (14). We detected the GTT, GAT and AGT mutations, corroborating previous reports that these mutations are common in pancreatic cancers (17, 18).

Theoretically, an FND-ECA chip can simultaneously detect multiple mutations of different types, including SNPs, deletions, insertions, translocations and short tandem repeats. For example, alterations in the *p53* tumor suppressor genes have been detected in 40-76% of pancreatic cancer tissues and mutational hot-spots are mainly located in exons 5 to 8 (19). Detection of *p53* in pancreatic cancer specimens by FND-ECA chip is now in progress in our laboratory. Our goal is to establish parallel analyses of multiple DNA targets in pancreatic cancer with the ECA chip to develop an automated analytic system for clinical use.

In conclusion, the FND-ECA chip provides a sensitive, rapid and reliable screening assay for the detection of point mutations in a variety of clinical samples and is, therefore, suitable for use as a screening method.

Acknowledgements

This study was supported in part by a Grant-in-Aid for Scientific Research from the New Energy and Industrial Technology Development Organization (NEDO), Japan, a Grant-in-Aid for Research on Advanced Medical Technology from the Japanese Ministry of Health, Labor and Welfare, and Grants-in-Aid for Scientific Research on Priority Areas from the Ministry of Education, Science, Sports and Culture of Japan.

References

1 Epstein JR, Biran I and Walt DR: Fluorescence-based fibre optic arrays: a universal platform for sensing. Chem Soc Rev *32*: 203-214, 2003.

2 Wang J: Electroanalysis and biosensors. Anal Chem *71*: 328R-332R, 1999.

3 Wang J: Electroanalysis and biosensors. Anal Chim Acta *469*: 63-71, 2002.

4 Drummond TG, Hill MG and Barton JK: Electrochemical DNA sensors. Nat Biotechnol *21*: 1192-1199, 2003.

5 Yamashita K, Takenaka S and Takagi M: Highly sensitive detection of target gene by electrochemical method. Nucleic Acids Symp Ser *42*: 185-186, 1999.

6 Takenaka S, Yamashita K, Takagi M *et al*: DNA sensing on a DNA probe-modified electrode using ferrocenylnaphthalene diimide as the electrochemically active ligand. Anal Chem *72*: 1334-1341, 2000.

7 Takenaka S: Highly sensitive probe for gene analysis by electrochemical approach. Bull Chem Soc Jpn *74*: 217-224, 2000.

8 Yamashita K, Takagi M, Kondo H *et al*: Electrochemical detection of nucleic base mismatches with ferrocenyl naphthalene diimide. Anal Biochem *306*: 188-196, 2002.
9 Nojima T, Yamashita K, Takagi A *et al*: Direct detection of single nucleotide polymorphism (SNP) with genomic DNA by the ferrocenylnaphthalene diimide-based electrochemical hybridization assay (FND-EHA). Anal Sci *19*: 79-83, 2003.
10 Sato S, Maeda Y, Nojima T *et al*: SNP analysis by using ferrocenyl naphthalene diimide (FND)-based electrochemical hybridization assay (EHA). Nucleic Acids Res Suppl *3*: 169-170, 2003.
11 Coppola D: Molecular prognostic markers in pancreatic cancer. Cancer Control *7*: 421-427, 2000.
12 MacKenzie MJ: Molecular therapy in pancreatic adenocarcinoma. Lancet Oncol 5: 541-549, 2004.
13 Mizumoto K and Tanaka M: Genetic diagnosis of pancreatic cancer. J Hepatobiliary Pancreat Surg *9*: 39-44, 2002.
14 Trumper L, Menges M, Daus H *et al*: Low sensitivity of the ki-ras polymerase chain reaction for diagnosing pancreatic cancer from pancreatic juice and bile: a multicenter prospective trial. J Clin Oncol *20*: 4331-4337, 2002.
15 Sambrock J, Fritsh EF and Maniatis T: Molecular Cloning: A Laboratory Manual. Cold Spring Harbor Laboratry Press, New York: Wiley-Liss, 1989.
16 Wakai J, Takagi A, Nakayama M *et al*: A novel method of identifying genetic mutations using an electrochemical DNA array. Nucleic Acids Res *32*: e141, 2004.
17 Hruban RH, van Mansfeld AD, Offerhaus GJ *et al*: *K-ras* oncogene activation in adenocarcinoma of the human pancreas. A study of 82 carcinomas using a combination of mutant-enriched polymerase chain reaction analysis and allele-specific oligonucleotide hybridization. Am J Pathol *143*: 545-554, 1993.
18 Mariyama M, Kishi K, Nakamura K *et al*: Frequency and types of point mutation at the 12th codon of the *c-Ki-ras* gene found in pancreatic cancers from Japanese patients. Jpn J Cancer Res *80*: 622-626, 1989.
19 Miyahara H, Yamashita K, Knai M *et al*: Electrochemical analysis of single nucleotide polymorphisms of p53. Talanta *56*: 829-835, 2002.

Received October 19, 2005
Accepted December 12, 2005

Nuclear Factor-κB Contributes to Hedgehog Signaling Pathway Activation through Sonic Hedgehog Induction in Pancreatic Cancer

Hiroshi Nakashima,[1] Masafumi Nakamura,[1] Hiroshi Yamaguchi,[2] Naoki Yamanaka,[1] Takashi Akiyoshi,[1] Kenichiro Koga,[1] Koji Yamaguchi,[3] Masazumi Tsuneyoshi,[2] Masao Tanaka,[3] and Mitsuo Katano[1]

Departments of [1]Cancer Therapy and Research, [2]Anatomic Pathology, and [3]Surgery and Oncology, Graduate School of Medical Sciences, Kyushu University, Fukuoka, Japan

Abstract

The hedgehog (Hh) signaling pathway, which functions as an organizer in embryonic development, is implicated in the development of various tumors. In pancreatic cancer, pathway activation is reported to result from aberrant expression of the ligand, sonic Hh (Shh). However, the details of the mechanisms regulating Shh expression are not yet known. We hypothesized that nuclear factor-κB (NF-κB), a hallmark transcription factor in inflammatory responses, contributes to the overexpression of Shh in pancreatic cancer. In the present study, we found a close positive correlation between NF-κB p65 and Shh expression in surgically resected pancreas specimens, including specimens of chronic pancreatitis and pancreatic adenocarcinoma. We showed that blockade of NF-κB suppressed constitutive expression of *Shh* mRNA in pancreatic cancer cells. Further activation of NF-κB by inflammatory stimuli, including interleukin-1β, tumor necrosis factor-α, and lipopolysaccharide, induced overexpression of Shh, resulting in activation of the Hh pathway. Overexpression of Shh induced by these stimuli was also suppressed by blockade of NF-κB. NF-κB-induced Shh expression actually activated the Hh pathway in a ligand-dependent manner and enhanced cell proliferation in pancreatic cancer cells. In addition, inhibition of the Hh pathway as well as NF-κB suppressed the enhanced cell proliferation. Our data suggest that NF-κB activation is one of the mechanisms underlying Shh overexpression in pancreatic cancer and that proliferation of pancreatic cancer cells is accelerated by NF-κB activation in part through Shh overexpression. (Cancer Res 2006; 66(14): 7041-9)

Introduction

Pancreatic cancer is one of the most lethal of all malignancies. Therapeutic options for patients with unresectable, metastatic, or recurrent disease are extremely limited, and few patients survive for 5 years, which underscores the need for new therapies (1, 2). A better understanding of the mechanisms that underlie development of pancreatic cancer would help to identify novel molecular targets for treatment.

Requests for reprints: Mitsuo Katano, Department of Cancer Therapy and Research, Graduate School of Medical Sciences, Kyushu University, 3-1-1 Maidashi, Higashi-ku, Fukuoka 812-8582, Japan. Phone: 81-92-642-6941; Fax: 81-92-642-6221; E-mail: mkatano@tumor.med.kyushu-u.ac.jp.

doi:10.1158/0008-5472.CAN-05-4588

The hedgehog (Hh) signaling pathway is crucial to growth and patterning in a wide variety of tissues during embryonic development (3, 4). Of three Hh ligands, sonic Hh (Shh), Indian Hh (Ihh), and desert Hh (Dhh), Shh is reported to play an essential role in the development of pancreatic cancer as well as pancreatic organogenesis (5, 6). Shh undergoes extensive post-translational modifications to become biologically active (7). The signal peptide is cleaved from the precursor form of Shh to yield the 45-kDa full-length form. Further processing of this molecular form of Shh generates a 19-kDa amino and 26-kDa COOH-terminal peptides. The 19-kDa NH_2-terminal peptide undergoes COOH-terminal esterification to a cholesterol molecule before being secreted into the extracellular spaces where it mediates the physiologic actions of Shh (8). The response to Shh is mediated by two transmembrane proteins, Smoothened (Smo) and Patched (Ptc), and by downstream transcription factors that are members of the Gli family. In the absence of Shh, Ptc suppresses the signaling activity of Smo. When Shh binds Ptc, Ptc is inactivated, enabling signaling via Smo. Smo releases the transcription factor Gli from a large protein complex, and Gli translocates to the nucleus to activate Hh target genes, including *Ptc1* (3, 4). It has been reported that the plant-derived teratogenic steroidal alkaloid cyclopamine inhibits the Hh pathway by antagonizing Smo (9).

Recently, ligand-dependent activation of the Hh pathway, especially due to aberrant expression of its ligand, Shh, has been detected in pancreatic cancer, and cyclopamine suppresses the growth of pancreatic cancer cells both *in vitro* and *in vivo* (10). These findings suggest that the Hh pathway may be a viable therapeutic target for treatment of pancreatic cancer, but it remains unclear how Shh is regulated in pancreatic cancer (11). One clue toward identification of the factors regulating Shh is the similarity between cancer development and tissue repair, a late phase of inflammation. It has been reported that, during repair of bronchial epithelium, transient activation of the Hh pathway occurs within the normally quiescent bronchial epithelium, and such a process may well occur during adult gut epithelial turnover (12, 13).

Association between chronic inflammation and the development of cancer has been recognized for several years (14–18). Various cytokines, such as tumor necrosis factor-α (TNF-α) and interleukin-1 (IL-1), which seem to play roles in inflammatory responses and the fibrotic reaction, are overexpressed in pancreatic cancer (19–21). Most of these cytokines are potent activators of nuclear factor-κB (NF-κB), which has been reported to be also activated in pancreatic cancer (22, 23). NF-κB is a transcription factor that controls expression of numerous genes involved in inflammation and immune response processes, including proliferation, invasion

and adhesion, angiogenesis, and apoptosis (22). In most unstimulated, normal cells, NF-κB is present in the cytoplasm as an inactive heterodimer composed of the p50, p65, and IκBα subunits. After activation, IκBα undergoes phosphorylation and ubiquitination-dependent degradation by the proteasome. Consequently, nuclear localization signals on the p50-p65 heterodimer are exposed, leading to nuclear translocation and binding to a specific consensus sequence that activates gene transcription, including genes encoding inflammatory cytokines, chemokines, growth factors, cell adhesion molecules, and cytokine receptors (24).

In the present study, we hypothesized that NF-κB activation upregulates expression of Shh, resulting in activation of Hh signaling in pancreatic cancer. We first investigated the expression of both NF-κB and Shh in clinical samples of pancreas. We then examined the effect of NF-κB activity on Shh expression and Hh pathway activation in pancreatic cancer cells. Finally, we explored the biological significance of the correlation between NF-κB and activation of the Hh pathway in proliferation of pancreatic cancer cells.

Materials and Methods

Cell culture, reagents, and antibodies. Two human pancreatic ductal adenocarcinoma (PDAC) cell lines (AsPC-1 and SUIT-2; ref. 25) and Cos7, an SV40-immortalized monkey kidney cell line, were maintained in RPMI 1640 (Life Technologies, Grand Island, NY) supplemented with 10% FCS (Life Technologies) and antibiotics [100 units/mL penicillin (Meijiseika, Tokyo, Japan) and 100 μg/mL streptomycin (Meijiseika), referred to as complete culture medium] at 37°C. Lipopolysaccharide (LPS) from *Escherichia coli* (B4), pyrrolidine dithiocarbamate (PDTC), and recombinant human IL-1β were purchased from Sigma (Deisenhofen, Germany). Recombinant human TNF-α was purchased from Dainippon Pharmaceutical (Osaka, Japan). Cyclopamine, purchased from Toronto Research Chemicals (North York, Ontario, Canada), was diluted in 100% methanol. Rabbit anti-NF-κB p65 (sc-109) and anti-Shh (sc-9024) antibodies were purchased from Santa Cruz Biotechnology (Santa Cruz, CA). Rabbit anti-β-actin antibody and rat anti-Shh NH_2-terminal peptide antibody were purchased from Biomedical Technologies (Stoughton, MA) and R&D Systems (Minneapolis, MN), respectively.

Clinical samples and immunohistochemistry. Surgical specimens were obtained from six patients with a benign pancreatic endocrine cell tumor, eight with chronic pancreatitis, and six with PDAC, all of whom underwent resection at the Department of Surgery and Oncology, Kyushu University (Fukuoka, Japan). All patients gave informed consent. Samples were fixed in 10% formalin and embedded in paraffin. For immunostaining of clinical samples, single-antibody detection was accomplished as described previously (26). In brief, all primary antibodies were incubated overnight at 4°C. Secondary antibodies were applied for 1 hour at room temperature. Immune complexes were visualized with 3,3′-diaminobenzidine as chromogen. Slides were counterstained with hematoxylin. The intensity of p65 staining of the pancreatic duct epithelium or cancer cells was scored according to the predominant pattern as 0, negative (weak or similar to background); 1, weak (less intense than adjacent acini); 2, moderate (similar intensity to adjacent acini); and 3, strong (stronger than adjacent acini). Ten pancreatic ducts or cancer nests in each section were scored, and the average score for each section was taken as the p65 staining score. For immunostaining of Shh, numbers of cytoplasmic-positive cells in pancreatic duct epithelium or cancer cells were counted. If the intensity of staining was similar to that of background staining, the staining was judged as negative. Five hundred cells were counted, and the percentage of Shh-positive cells was calculated for each section.

Plasmids, oligodeoxynucleotides, and cell transduction. Phosphorothioated and double-stranded NF-κB decoy oligodeoxynucleotides, 5′-CCTTGAAGGGATTTCCCTCC-3′, and scramble oligodeoxynucleotides, 5′-TTGCCGTACCTGACTTAGCC-3′, were purchased from Hokkaido System Science (Sapporo, Japan). Cells were transfected with 0.5 μmol/L NF-κB decoy or scramble oligodeoxynucleotides with LipofectAMINE (Life Technologies, Inc., Gaithersburg, MD) according to the manufacturer's instructions. Transfected cells were used for experiments 48 hours after transfection. pIRES2-hSHH-EGFP (referred to as pSHH-GFP) and pcDNA3.1/His-hGli1 (referred to as pGli1) were kindly provided by Dr. Aubie Shaw (Division of Urology, Department of Surgery, University of Wisconsin, Madison, WI; ref. 27) and Dr. H. Sasaki (Center for Developmental Biology, RIKEN, Kobe, Japan; ref. 28), respectively. pCMV-IκBα wild-type (WT) and pCMV-IκBα mutant were purchased from BD Biosciences/Clontech (Palo Alto, CA). Cells seeded in six-well plates were transfected with 2 μg plasmid with TransFast reagent (Promega, Madison, WI) per manufacturer's protocol. Cells were used for experiments 48 hours after transfection. To collect control medium and Shh-rich medium, Cos7 cells were transfected with 2 μg pGFP and pSHH-GFP, respectively, with Superfect reagent (Qiagen, Valencia, CA) according to the manufacturer's instructions. Supernatant was collected 48 hours later and dissolved in complete culture medium at a 1:10 dilution. The supernatant from cells transfected with pSHH-GFP was called Shh-rich medium, whereas supernatants from cells transfected with pGFP were collected as control medium.

Luciferase assay. Cells in six-well plates were transfected with plasmids with Superfect transfection reagent according to the manufacturer's instructions. Cells on each well were cotransfected with 5 ng pRL-SV40 (Promega) and 2 μg pELAM-Luc (29), the NF-κB-dependent luciferase reporter (kindly provided by Dr. K. Takeda, Division of Embryonic and Genetic Engineering, Medical Institute of Bioregulation, Kyushu University). After 24 hours of pretreatment with PDTC or cyclopamine, IL-1β or TNF-α was added to each well, and luciferase assays were done 6 hours later with the dual luciferase assay kit (Promega) according to the manufacturer's instructions. The luciferase activities were normalized to the *Renilla* luciferase activity. For cotransfection of reporter plasmids and effector plasmids or oligodeoxynucleotidess, we transfected cells with 1 μg of each plasmid (cells were transfected with a total of 2 μg plasmid mixture). Luciferase assays were done 48 hours after transfection as described above.

Real-time reverse transcription-PCR. Total RNA was extracted by the guanidinium isothiocyanate-phenol-chloroform extraction method (30) and quantified by spectrophotometry (Ultrospec 2100 Pro, Amersham Pharmacia Biotech, Cambridge, United Kingdom). RNA (1 μg) was treated with DNase and reverse transcribed to cDNA with the Quantitect Reverse Transcription kit (Qiagen) according to the manufacturer's protocol. Reactions were run with iQ SYBR Green Supermix (Bio-Rad, Hercules, CA) on a DNA Engine Opticon 2 System (MJ Research, Waltham, MA). cDNA, prepared from AsPC-1 and SUIT-2 cells transfected with pSHH-GFP, were serially diluted in 10-fold increments and amplified in parallel with the various primer pairs to generate standard curves. Each sample was run in triplicate. All primer sets amplified fragments <200 bp long. Sequences of the primers used were β-actin forward, 5′-TTGCCGACAG-GATGCAGAAGGA-3′, and reverse, 5′-AGGTGGACAGCGAGGCCAGGAT-3′; Shh forward, 5′-GTGTACTACGAGTCCAAGGCAC-3′, and reverse, 5′-AGG-AAGTCGCTGTAGAGCAGC-3′; and Ptc1 forward, 5′-ATGCTGGCGGGATCT-GAGTTCGACT-3′, and reverse, 5′-GGGTGTGGGCAGGCGGTTCAAG-3′. The amount of each target gene in a given sample was normalized to the level of β-actin in that sample.

Immunoblotting. Whole-cell extraction was done with M-PER Reagents (Pierce Biotechnology, Rockford, IL) according to the manufacturer's instructions. Protein concentration was determined with a Bio-Rad Protein Assay (Bio-Rad). Whole-cell extract (100 μg) was separated by electrophoresis on 12.5% SDS-polyacrylamide gel and transferred to Protran nitrocellulose membranes (Schleicher & Schnell BioScience, Dassel, Germany). Blots were then incubated with anti-Shh (1:100) or anti-β-actin (1:500) primary antibody overnight at 4°C. Blots were incubated with horseradish peroxidase–linked anti rabbit IgG antibody (Amersham Biosciences, Piscataway, NJ) at room temperature for 1 hour. Immunocomplexes were detected with an enhanced chemiluminescence reagent (Amersham Biosciences) and visualized with a Molecular Imager FX (Bio-Rad).

Proliferation assay. Cells (2×10^3 per well) seeded in 48-well plates in complete culture medium were incubated overnight. Medium was changed to RPMI 1640 with 0.8% FCS with or without 0.1 μg/mL LPS, 0.1 IU/mL TNF-α, or 0.1 ng/mL IL-1β in the presence or the absence of 0.3 μmol/L PDTC, 5 μg/mL anti-Shh NH_2-terminal peptide antibody, or 5 μmol/L cyclopamine. To test for the effects of Shh-rich medium on the cell proliferation, medium was changed to control or Shh-rich medium. After 4 days of incubation, cells were harvested by trypsinization, and cells were counted with a Coulter counter (Beckman Coulter, Fullerton, CA). When transfection was needed, cells (8×10^3 per well) seeded in 48-well plates were transfected with 0.8 μg pSHH-GFP or 0.4 μg pGli1 with Transfast reagent. Transfected cells were incubated in complete medium for 16 hours, and the medium was changed to RPMI 1640 with 0.8% FCS and manipulated as described above.

Electrophoretic mobility shift assay. Electrophoretic mobility shift assay (EMSA) was done as reported previously (30, 31). Nuclear extract (10 μg) was incubated for 30 minutes at 37°C with binding buffer [60 mmol/L HEPES (pH 7.5), 180 mmol/L KCl, 15 mmol/L MgCl2, 0.6 mmol/L EDTA, 24% glycerol], poly(deoxyinosinic-deoxycytidylic acid), and ^{32}P-labeled double-stranded oligonucleotide containing the binding motif of NF-κB (Promega). The sequence of the double-stranded oligomer used for EMSA was 5′-AGTTGAGGGGACTTTCCCAGGC-3′. The reaction mixtures were loaded onto a 4% polyacrylamide gel and electrophoresed with a running buffer of 0.25% Tris-borate EDTA. Gel being dried, the DNA-protein complexes were visualized by autoradiography.

Statistical analysis. Student's *t* test was used for statistical analysis. The relations between variables were assessed with Spearman rank correlation coefficient. A $P < 0.05$ was considered significant.

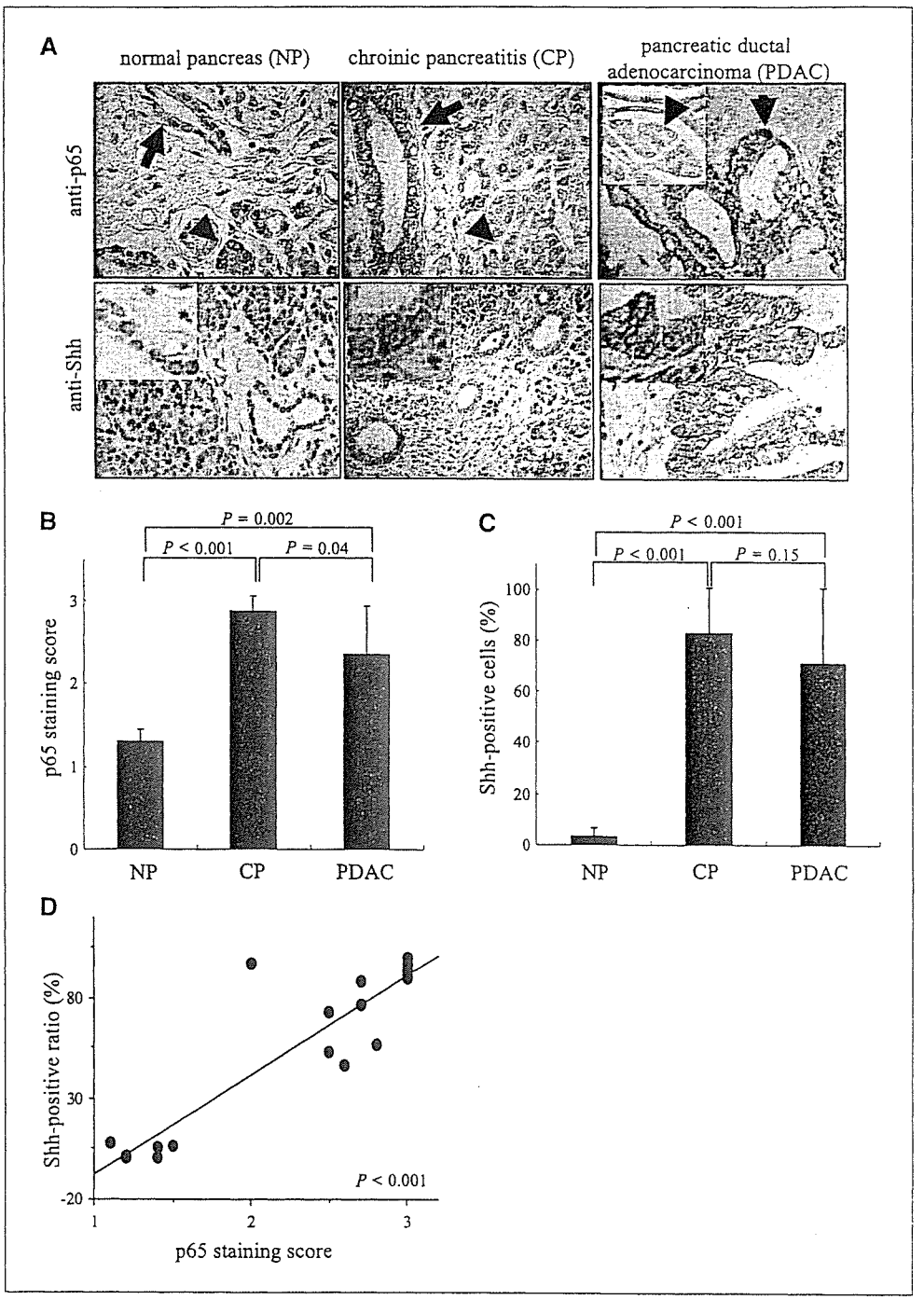

Figure 1. Expression of NF-κB p65 and Shh in human pancreatic tissues. *A, top,* p65 expression by duct epithelium (*arrow*) is less intense than that by adjacent acinar cells (*arrowhead*) in normal pancreatic tissue (*NP*). P65 expression by duct epithelium is stronger than that by adjacent acinar cells in chronic pancreatitis (*CP*). P65 expression by PDAC cells is stronger than that in acinar cells in normal pancreas in the same section. *Bottom,* few duct epithelium cells in normal pancreatic tissues showed immunoreactivity for Shh, whereas most duct epithelium cells in chronic pancreatitis and cancer cells in PDAC express Shh. Magnification, ×200. *Inset,* magnification, ×400. *B,* the intensity of p65 staining of the pancreatic duct epithelium (normal pancreas and chronic pancreatitis) or cancer cells (PDAC) was scored as described in Materials and Methods. *C,* the number of immunoreactive cells for Shh in pancreatic duct epithelium (normal pancreas and chronic pancreatitis) or cancer cells (PDAC) was counted. *D,* p65 staining score and Shh-positive cell ratio (%). The relations among the variables were assessed with the Spearman rank correlation coefficient.

Results

Shh expression correlated positively with NF-κB activation in specimens of human pancreas. To examine whether NF-κB activation was associated with expression of Hh pathway components in clinical samples, we stained a series of 20 paraffin-embedded specimens, including 6 specimens of normal pancreas from resected benign pancreatic tumors, 8 specimens of chronic pancreatitis, and 6 specimens of PDAC, which had normal pancreatic structures in the same section. Expression of the functional component of NF-κB, p65 (Fig. 1*A*, *top*), and Shh (Fig. 1*A*, *bottom*) was examined immunohistochemically. We then scored the intensity of p65 immunostaining of pancreatic duct epithelium (normal pancreas and chronic pancreatitis) or cancer cell (pancreatic cancer). The p65 staining scores (mean ± SE) of pancreatic duct epithelium in normal pancreas and chronic pancreatitis and of cancer cells in PDAC were 1.3 ± 0.15, 2.88 ± 0.19, and 2.37 ± 0.56, respectively (Fig. 1*B*). Chronic pancreatitis and PDAC showed significantly higher scores than these of normal pancreas. The percentage of cells with cytoplasmic staining of Shh (mean ± SE) was 3.4 ± 3.3% in normal pancreas, 82.5 ± 17.9% in chronic pancreatitis, and 70.8 ± 29.7% in PDAC (Fig. 1*C*). The Shh-positive staining ratios of chronic pancreatitis and PDAC were significantly higher than the ratio of normal pancreas. In addition, when all specimens were included, a strong positive correlation was detected between the p65 staining score and the Shh-positive staining ratio (Fig. 1*D*). These data suggested that there was a correlation between NF-κB activation and Shh expression in clinical specimens of pancreas.

Expression of *Shh* mRNA correlated positively with NF-κB activity in cultured pancreatic cancer cells. To clarify the relation between *Shh* mRNA expression and NF-κB activity observed in our clinical study, we did *in vitro* experiments with two human pancreatic cancer cell lines, AsPC-1 and SUIT-2 (25). We confirmed that both cell lines showed increased NF-κB DNA-binding activity by EMSA and that they constitutively expressed *Shh*, *Ptc1*, and *Gli1* at both mRNA and protein levels (data not

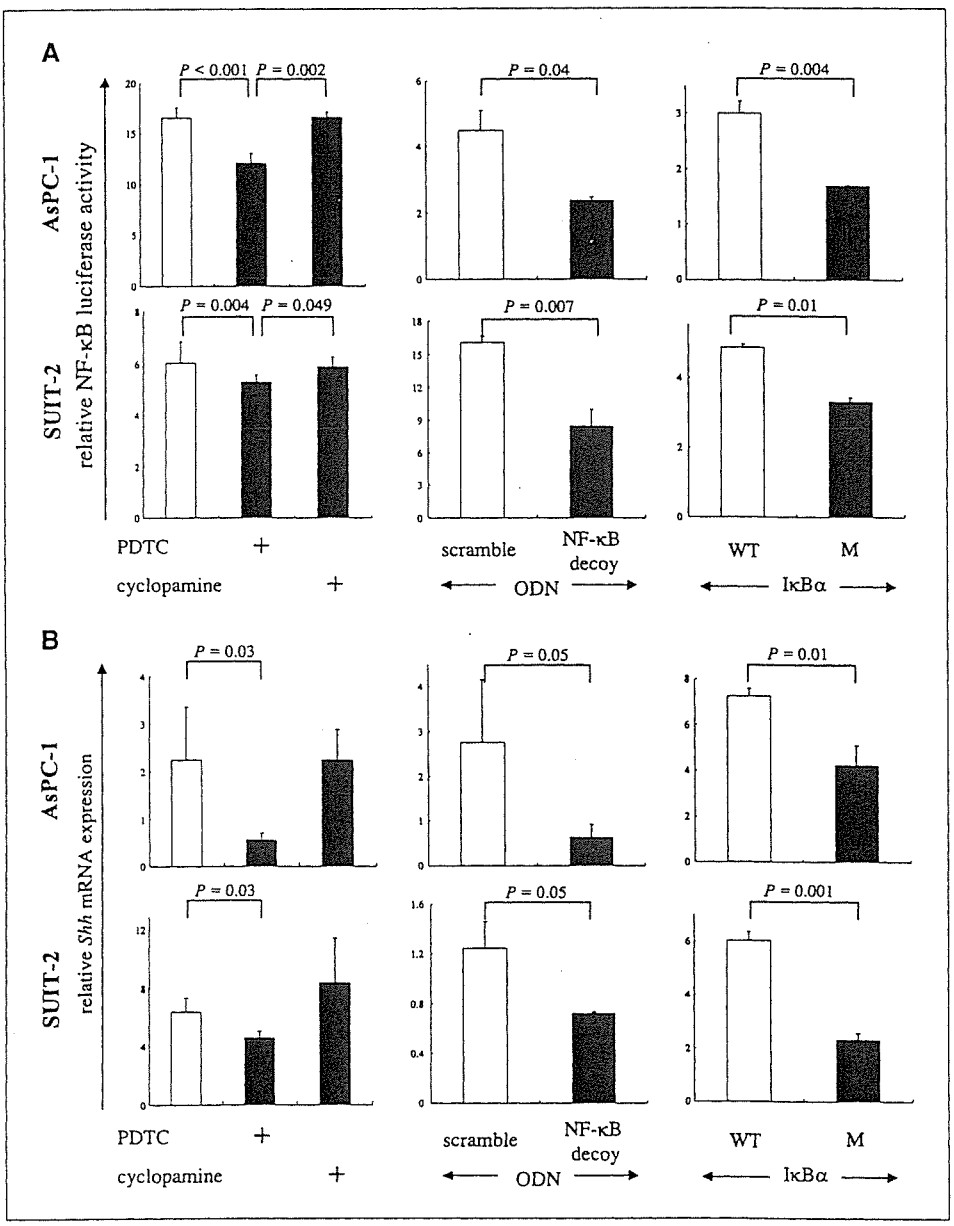

Figure 2. Effects of NF-κB inhibitors on NF-κB transcriptional activity and *Shh* mRNA expression in pancreatic cancer cells. *A*, dual luciferase assay was done 6 hours after adding 10 IU/mL of TNF-α. Relative NF-κB luciferase activity after normalization to *Renilla* luciferase activity. *Columns*, mean of triplicate experiments; *bars*, SD. *Left*, cells were pretreated for 24 hours with 10 μmol/L PDTC or cyclopamine 24 hours after transfection with reporter plasmids; *middle*, scramble or NF-κB decoy oligodeoxynucleotides and reporter plasmids were cotransfected for 48 hours; *right*, IκBα WT or IκBα mutant (*M*) plasmid and reporter plasmids were cotransfected for 48 hours. *B*, *Shh* mRNA expression by AsPC-1 and SUIT-2 cells was examined with real-time RT-PCR. Relative *Shh* mRNA level after normalization to the corresponding β-actin mRNA expression. *Columns*, mean of three independent experiments; *bars*, SD. *Left*, cells were treated with 10 μmol/L PDTC or cyclopamine for 24 hours; *middle*, relative *Shh* mRNA levels were assessed 48 hours after transfection of oligodeoxynucleotidess; *right*, relative *Shh* mRNA levels were assessed 48 hours after transfection of oligodeoxynucleotidess, IκBα WT, or IκBα mutant.

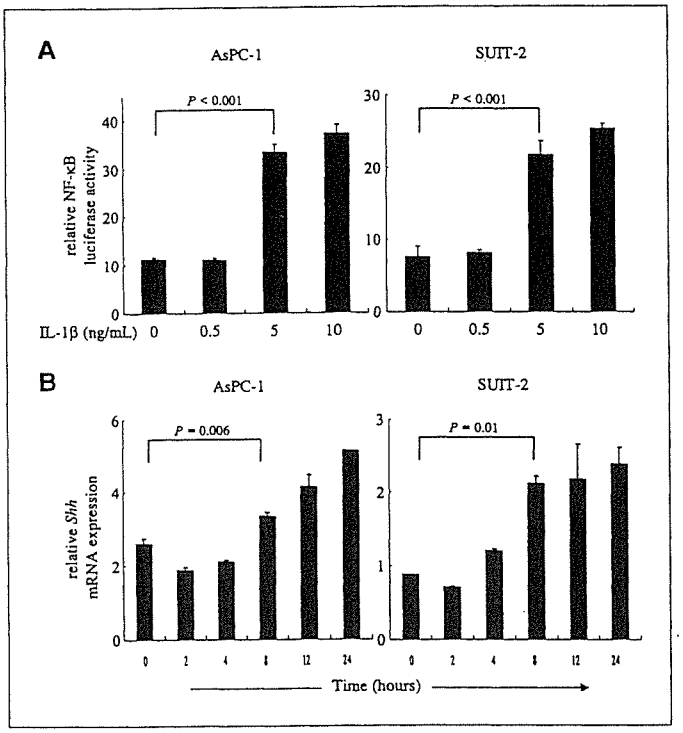

Figure 3. IL-1β enhances expression of *Shh* mRNA by pancreatic cancer cells. *A*, AsPC-1 and SUIT-2 cells were treated with IL-1β for 6 hours, and dual luciferase assay was done as described. *B*, *Shh* mRNA expression was examined by real-time RT-PCR after cells were exposed to 5 ng/mL IL-1β.

shown). We first examined whether inhibition of NF-κB activity altered Shh expression in these cell lines. We treated both cell lines with PDTC for 24 hours to inhibit NF-κB activity (30). Transcription activity of NF-κB and expression of *Shh* mRNA were examined by NF-κB reporter assay and real-time reverse transcription-PCR (RT-PCR), respectively. PDTC significantly inhibited NF-κB transcriptional activity in both cell lines (Fig. 2*A*, *left*). Constitutive expression of *Shh* mRNA in these cell lines was reduced significantly in parallel with NF-κB activity (Fig. 2*B*, *left*), suggesting that inhibition of NF-κB activity reduced constitutive expression of *Shh* mRNA in pancreatic cancer cells. In contrast, the Hh pathway inhibitor, cyclopamine, had no effect on NF-κB transcriptional activity or *Shh* mRNA expression in these cells (Fig. 2*A* and *B*, *left*).

To confirm these results, we transfected both cell lines with NF-κB decoy oligodeoxynucleotides to suppress NF-κB activity as reported previously (31). When transfected with NF-κB decoy oligodeoxynucleotides, NF-κB-dependent reporter activity of AsPC-1 and SUIT-2 cells decreased to 52.7% and 51.6%, respectively, that of the scramble oligodeoxynucleotides control (Fig. 2*A*, *middle*). Expression of *Shh* mRNA in AsPC-1 and SUIT-2 cells transfected with NF-κB decoy oligodeoxynucleotides was decreased to 23.2% and 58.3%, respectively, that of the scramble oligodeoxynucleotides (Fig. 2*B*, *middle*). Furthermore, we transfected both cell lines with pCMV-IκBα mutant, which was reported to have a dominant-negative effect on NF-κB activity (32). Transfection of IκBα mutant significantly suppressed NF-κB transcriptional activity in both cell lines (Fig. 2*A*, *right*). When cells were transfected with IκBα mutant, constitutive expression of *Shh* mRNA by AsPC-1 and SUIT-2 cells was reduced significantly to 58.1% and 37.7%, respectively, that of cells when transfected with IκBα WT (Fig. 2*B*, *right*). These data showed that inhibition of NF-κB activity resulted in reducing the constitutive expression of *Shh* mRNA in pancreatic cancer cells.

We next examined whether further activation of NF-κB could induce overexpression of *Shh* mRNA in pancreatic cancer cells. We used one of the proinflammatory cytokines, IL-1β, as a NF-κB activator because it has been reported that IL-1β causes constitutive NF-κB activation in pancreatic cancer cells (33). IL-1β (5 ng/mL) significantly enhanced NF-κB activity in both cell lines (Fig. 3*A*). When cells were treated with 5 ng/mL IL-1β, significantly enhanced expression of *Shh* mRNA was observed in these cell lines after 8 hours (Fig. 3*B*). Taken together, these data suggested that NF-κB activity affected *Shh* expression by pancreatic cancer cells.

Shh protein level depended on NF-κB activity in pancreatic cancer cells. To confirm that the Shh protein level is correlated with NF-κB activity in pancreatic cancer cells, we did immunoblotting. The Shh protein level was quantified with the 19-kDa fragment because it is the physiologic form of Shh (8, 34). We first treated pancreatic cancer cells with 5 ng/mL IL-1β and examined whether NF-κB activation altered the Shh protein level. As shown in Fig. 4*A*, IL-1β increased Shh levels in AsPC-1 and SUIT-2 cells. Furthermore, 1 IU/mL TNF-α and 10 μg/mL LPS, both of which are potent NF-κB activators, also enhanced expression of Shh protein (Fig. 4*A*). These findings indicated that NF-κB activation enhanced Shh protein production in these cell lines. We then investigated whether NF-κB inhibitors could reduce the enhanced protein level of Shh by IL-1β. When treated with IL-1β in

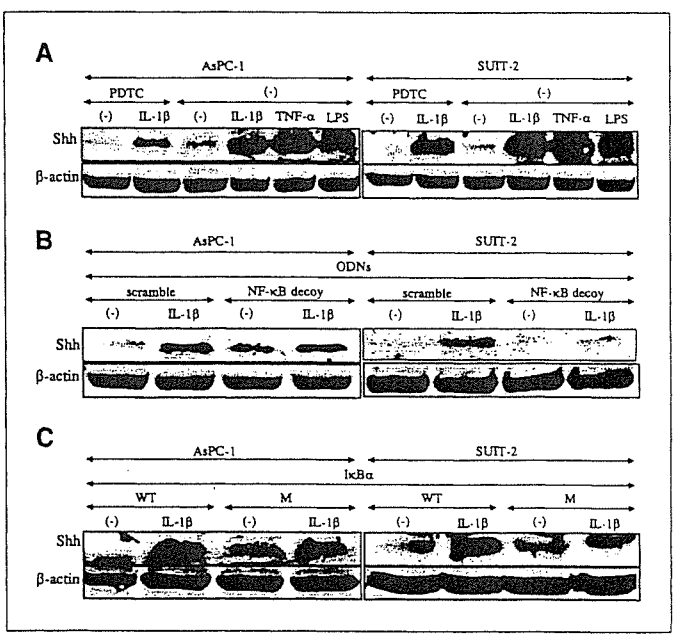

Figure 4. Level of Shh protein correlates with NF-κB activity in pancreatic cancer cells. Representative of three independent experiments. Whole-cell extract (100 μg) was resolved by electrophoresis on a 12.5% SDS-polyacrylamide gel and immunoblotted. *A*, AsPC-1 and SUIT-2 cells were treated with 5 ng/mL IL-1β, 10 μg/mL LPS, and 1 IU/mL TNF-α for 24 hours after they were pretreated with 10 μmol/L PDTC for 24 hours. *B*, AsPC-1 and SUIT-2 cells were transfected with 0.5 μmol/L of oligodeoxynucleotidess for 48 hours. After 24 hours of incubation with 5 ng/mL IL-1β, immunoblotting was done. *C*, AsPC-1 and SUIT-2 cells were transfected with IκBα WT or IκBα mutant plasmid for 24 hours. After 24 hours of incubation with 5 ng/mL IL-1β, immunoblotting was done.

the presence of NF-κB inhibitors, including PDTC (Fig. 4*A*), NF-κB decoy oligodeoxynucleotides (Fig. 4*B*), and IκBα mutant (Fig. 4*C*), protein levels of Shh were reduced. These data suggested that the Shh protein level was positively correlated with NF-κB activity in pancreatic cancer cells.

Overexpression of Shh induced by NF-κB activation led to enhanced Hh pathway activation in pancreatic cancer cells. We examined whether NF-κB-induced Shh could activate the Hh pathway because activation of this pathway was reported to be ligand dependent in pancreatic cancer, which means that the aberrant signaling must be mediated by Shh protein (35). To confirm that ligand-dependent Hh pathway activation occurs in AsPC-1 and SUIT-2 cells, the cells were transfected with pSHH-GFP to overexpress Shh, and the *Ptc1* mRNA level was then monitored by real-time RT-PCR. Because Ptc1 is a transcriptional target of the Hh pathway as well as a receptor in this pathway, the level of *Ptc1* mRNA reflects the degree of Hh pathway activity (11, 36). The transfection efficiency reached ~70% in both cell lines (data not shown). As shown in Fig. 5*A*, real-time RT-PCR revealed that cells transfected with pSHH-GFP expressed higher levels of *Shh* mRNA than were expressed by cells transfected with control plasmid (34- and 126-fold increases in AsPC-1 and SUIT-2 cells, respectively). Expression of *Ptc1* mRNA in pSHH-GFP-transfected cells was approximately 4.8- and 2.2 -fold higher in AsPC-1 and SUIT-2 cells, respectively, than on control-transfected cells (Fig. 5*A*). These data suggest that overexpression of Shh enhanced Hh pathway activation within the same cells.

We next examined whether IL-1β also activated the Hh pathway in these cell lines. When cells were treated with 5 ng/mL IL-1β, expression of *Ptc1* mRNA was increased 1.6-fold after 8 hours in AsPC-1 cells and 2.2-fold after 12 hours in SUIT-2 cells (Fig. 5*B*). These data suggested that IL-1β activated the Hh pathway through up-regulation of Shh in pancreatic cancer cells.

NF-κB activation up-regulated Shh and promoted proliferation of pancreatic cancer cells. We examined whether Shh and the Hh pathway could promote proliferation of pancreatic cancer cell lines. When AsPC-1 and SUIT-2 cells were transfected with vector expressing Gli1, a transcription factor in the Hh pathway, cell proliferation was 2.1- and 1.9-fold higher in pGli1-expressing cells, respectively, than in cells transfected with control plasmid, pcDNA3.1 (Fig. 6*A*, *top*). Proliferation of AsPC-1 and SUIT-2 cells transfected with pSHH-GFP was 1.9- and 1.8-fold higher, respectively, than that of cells transfected with pGFP (Fig. 6*A*, *bottom*). To confirm that the secreted Shh had autocrine effects on physiologic functions, we transfected Cos7 cells with pSHH-GFP and prepared Shh-rich medium. Immunoblotting confirmed that Shh-rich medium contained more Shh protein than control medium (data not shown). AsPC-1 and SUIT-2 cells incubated in Shh-rich medium proliferated more rapidly than those in control medium (Fig. 6*B*). In contrast, 10 μmol/L cyclopamine, a specific inhibitor of the Hh pathway, inhibited proliferation of these cell lines (Fig. 6*C*). Taken together, these findings indicated that Shh and the Hh pathway contributed to proliferation of these cell lines, which was consistent with previous reports (10).

Finally, we examined whether overexpression of Shh induced by inflammatory stimuli also stimulated proliferation of pancreatic cancer cells. When AsPC-1 and SUIT-2 cells were treated with 0.1 μg/mL LPS (Fig. 7*A*), 0.1 IU/mL TNF-α (Fig. 7*B*), and 1 ng/mL IL-1β (Fig. 7*C*), proliferation of both cell lines was significantly enhanced. As expected, the enhanced proliferation induced by each of these stimuli was blocked completely by PDTC (Fig. 7*A*; data not shown). Enhanced proliferation was also suppressed by anti-Shh neutralizing antibody (Fig. 7*B*; data not shown). Furthermore, enhanced proliferation was inhibited completely by cyclopamine (Fig. 7*C*; data not shown). These data suggest that inflammatory stimuli enhance proliferation of pancreatic cancer cells, at least in part, through overexpression of Shh, resulting in Hh pathway activation. To confirm these findings, both cell lines were cultured with PDTC. Proliferation of these cell lines was significantly inhibited by PDTC (Fig. 7*D*). However, the repressive effect of PDTC on cell proliferation was reduced when these cells were transfected with pSHH-GFP (Fig. 7*D*). These data suggested that NF-κB activation enhanced proliferation of pancreatic cancer cells, at least in part, through up-regulation of Shh expression. Taken together, these data suggested that inflammatory stimuli activated NF-κB, which led to overexpression of Shh, resulting in activation of the Hh pathway and enhanced proliferation of pancreatic cancer cells.

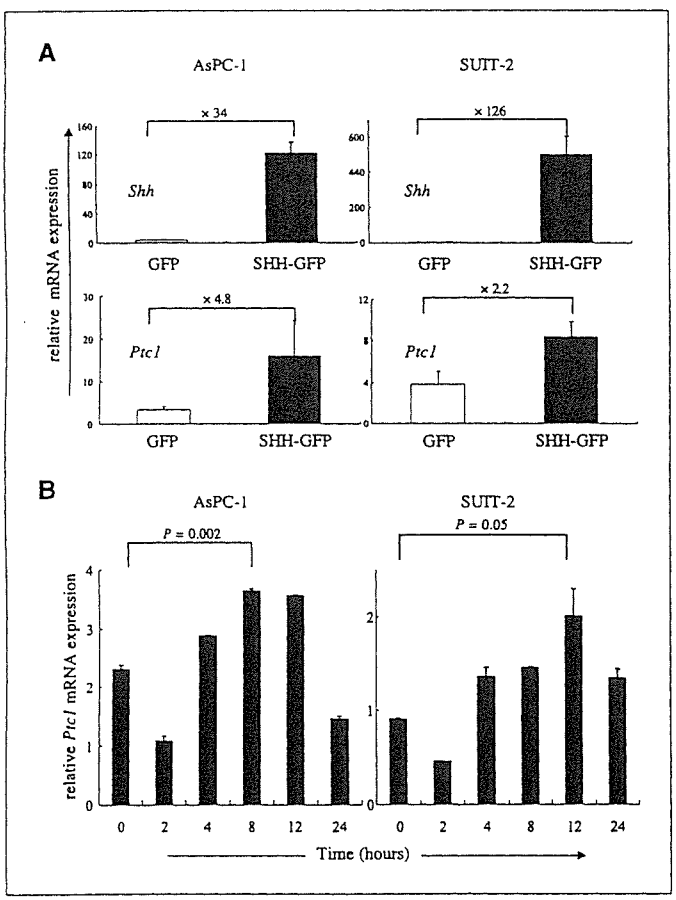

Figure 5. NF-κB activation and overexpression of Shh induce Hh pathway activation in pancreatic cancer cells. mRNA expression relative to that of corresponding *β-actin* mRNA expression. *Columns*, mean of three independent wells; *bars*, SD. *A*, cells were transfected with pGFP or pSHH-GFP for 24 hours, and then expression of *Shh* and *Ptc1* mRNAs was assessed by real-time RT-PCR. *B*, after adding 5 ng/mL IL-1β, relative *Ptc1* mRNA expression was determined with real-time RT-PCR.

Discussion

Here, we report for the first time that NF-κB contributes to Hh pathway activation through up-regulation of Shh expression in pancreatic cancer cells. There was a positive correlation between

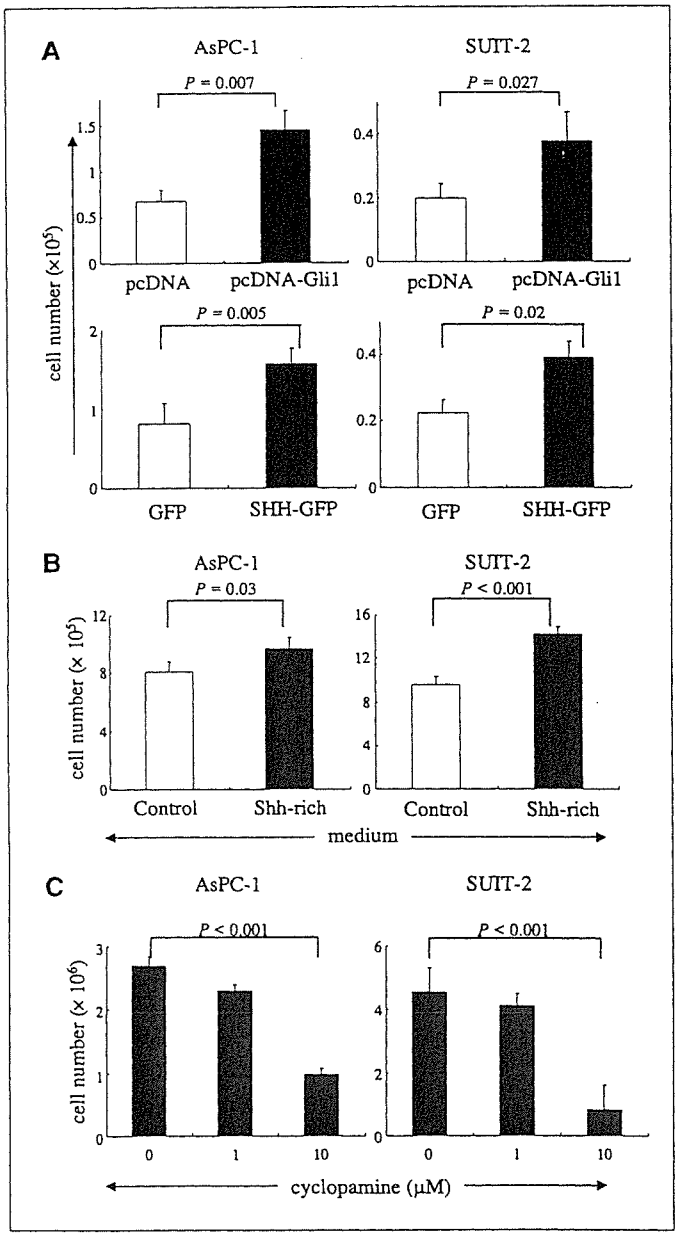

Figure 6. Ligand-dependent activation of the Hh pathway enhanced proliferation of pancreatic cancer cells. Proliferation assay was carried out in triplicate. *Columns*, mean of three independent experiments; *bars*, SD. *A*, cells in 48-well plates were transfected with 0.5 μg pcDNA3.1 or pcDNA3.1/Gli1 or 2 μg pGFP or pSHH-GFP, and cell numbers were determined after 4 days. *B*, numbers of AsPC-1 and SUIT-2 cells incubated in control medium or Shh-rich medium (as described in Materials and Methods) were counted after 4 days of incubation. *C*, cells were treated with 1 or 10 μmol/L cyclopamine for 4 days, and cell numbers were determined.

NF-κB and Shh expression in clinical tissue samples. Blockade of NF-κB suppressed constitutive *Shh* mRNA expression, whereas further activation of NF-κB induced overexpression of Shh *in vitro*. NF-κB-induced overexpression of Shh activated the Hh pathway in pancreatic cancer cells in a ligand-dependent manner, which resulted in enhanced cell proliferation.

It was recently reported that Hh pathway is constitutively activated in a variety of tumors and may play a crucial role during tumor development (5, 10, 11, 35). In some tumors, such as basal cell carcinomas and central nervous system tumors, active mutations of Shh, Smo, and Gli1 and loss-of-function mutations of Ptc1 can activate the Hh pathway (13, 37). In contrast, in cancers of the lung, breast, gastrointestinal tracts, and pancreas, activation of the Hh pathway is mediated by aberrant expression of its ligand, Shh (10, 11, 26). If so, it is important to elucidate the identities of the molecules that regulate expression of Shh. However, to our

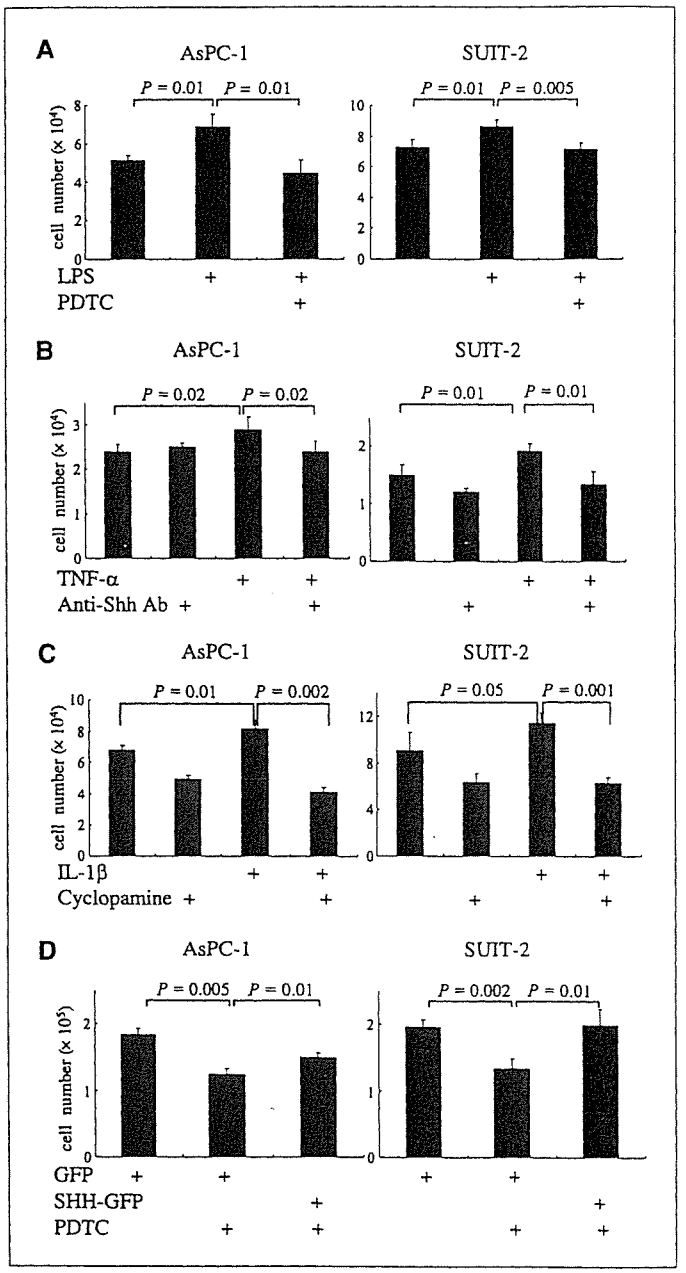

Figure 7. NF-κB activation induces proliferation of pancreatic cancer cells through overexpression of Shh and activation of the Hh pathway. Representative of three different experiments. Proliferation assay was carried out in triplicate. *Bars*, represent SD. *A*, cells were incubated in the presence of 0.1 μg/mL LPS with or without 0.3 μmol/L PDTC, and cell numbers were determined after 4 days. *B*, cells were incubated in the presence of 0.1 IU/mL TNF-α with or without 5 μg/mL anti-Shh neutralizing antibody, and cell numbers were determined after 4 days. *C*, cells were incubated in the presence of 0.1 ng/mL IL-1β with or without 5 μmol/L cyclopamine, and cell numbers were determined after 4 days. *D*, cells in 48-well plates were transfected with 2 μg pGFP or pSHH-GFP and incubated in complete medium overnight. Medium was changed to RPMI 1640 with 0.8% FCS with or without 0.3 μmol/L PDTC, and cell numbers were determined after 4 days.

knowledge, the detailed mechanisms that underlie up-regulation of expression of Shh in these tumors remain unclear (5, 10, 11, 35). Our present findings that NF-κB activation is one of the mechanisms responsible for Shh overexpression seem to have broad significance.

We focused on the role of NF-κB in Shh expression in pancreatic cancer for the following reasons. First, a close relationship between chronic inflammation and cancer development has been proposed (38). Second, NF-κB is one of the molecules responsible for the correlation between inflammation and cancer (22). Third, the Hh pathway has recently been regarded in adult tissue as a tissue repairing signal (13), and in general, tissue repairing signals seemed to be activated continuously in chronic inflammation.

Based on these findings, we hypothesized that NF-κB plays an important role in Hh pathway activation through induction of Shh expression in pancreatic cancer. As expected, a very close positive correlation between p65 and Shh expression was observed in clinical samples (Fig. 1*D*). We also observed that chronic pancreatitis specimens expressed high levels of Shh as well as NF-κB (Fig. 1*A-C*). Some reports have suggested that continuous Hh pathway activation could contribute to or promote carcinogenesis (10). Together with these results, our data raise a possibility that chronic pancreatitis provides such a setting via overexpression of NF-κB.

Using two PDAC cell lines, both of which showed constitutive NF-κB and Hh pathway activation (data not shown), we found that NF-κB contributes to Hh pathway activation in an autocrine manner through Shh induction. Three NF-κB inhibitors, which act at different points in the NF-κB pathway, all reduced Shh expression at both mRNA and protein levels (Figs. 2 and 4). Three inflammatory stimuli used as NF-κB activators, IL-1β, TNF-α, and LPS, all induced further activation of NF-κB in both cells (Figs. 2 and 3; data not shown). IL-1β and TNF-α have been reported to be causative molecules responsible for constitutive NF-κB activation in pancreatic cancer (38). Interestingly, LPS also induced NF-κB activation in these cells (data not shown). Although the detailed mechanism of NF-κB activation by LPS is unclear, both cells lines tested expressed Toll-like receptor 4, a main component of the LPS receptor complex (ref. 39; data not shown). These stimuli all increased expression of Shh protein (Fig. 4*A*). Increased expression of Shh was suppressed significantly by all three NF-κB inhibitors (Fig. 4; data not shown). We were also able to show that Shh induced by NF-κB activation is biologically active. NF-κB activation increased levels of the 19-kDa physiologically active form of Shh (Fig. 4), which activated the Hh pathway in an autocrine manner (Fig. 5) and enhanced cell proliferation (Fig. 7). Our data indicate a significant contribution of Shh induced by NF-κB activation to cell proliferation. Because cyclopamine is not specific inhibitor for Shh-induced Hh pathway activation, however, participation of other ligands, such as Ihh and Dhh in Hh pathway activation and cell proliferation cannot be excluded. In our system, an Hh pathway inhibitor, cyclopamine, had no effect on the transcriptional activity of NF-κB (Fig. 2*A*). We therefore believe that the Hh pathway has little effect on NF-κB activation.

In conclusion, in pancreatic cancer, overexpression of Shh results, at least in part, from constitutive activation of NF-κB; however, it remains to be determined whether NF-κB regulates Shh expression through a direct or indirect interaction. This novel finding that NF-κB influences Shh expression improves our understanding of the mechanism of Hh signaling activation in pancreatic cancer.

Acknowledgments

Received 1/2/2006; revised 4/11/2006; accepted 4/20/2006.

Grant support: General Scientific Research grants 16591326 and 17591414 and Ministry of Education, Culture, Sports, and Technology of Japan.

The costs of publication of this article were defrayed in part by the payment of page charges. This article must therefore be hereby marked *advertisement* in accordance with 18 U.S.C. Section 1734 solely to indicate this fact.

References

1. Li D, Xie K, Wolff R, et al. Pancreatic cancer. Lancet 2004;363:1049–57.
2. Bardeesy N, DePinho RA. Pancreatic cancer biology and genetics. Nat Rev Cancer 2002;2:897–909.
3. Hebrok M. Hedgehog signaling in pancreas development. Mech Dev 2003;120:45–57.
4. Cohen MM, Jr. The hedgehog signaling network. Am J Med Genet 2003;123:5–28.
5. Heiser PW, Hebrok M. Development and cancer: lessons learned in the pancreas. Cell Cycle 2004;3:270–2.
6. Wetmore C. Sonic hedgehog in normal and neoplastic proliferation: insight gained from human tumors and animal models. Curr Opin Genet Dev 2003;13:34–42.
7. Lee JJ, Ekker SC, von Kessler DP, et al. Autoproteolysis in hedgehog protein biogenesis. Science 1994;266:1528–37.
8. Bumcrot DA, Takada R, McMahon AP. Proteolytic processing yields two secreted forms of sonic hedgehog. Mol Cell Biol 1995;15:2294–303.
9. Chen JK, Taipale J, Cooper MK, et al. Inhibition of Hedgehog signaling by direct binding of cyclopamine to Smoothened. Genes Dev 2002;16:2743–8.
10. Thayer SP, di Magliano MP, Heiser PW, et al. Hedgehog is an early and late mediator of pancreatic cancer tumorigenesis. Nature 2003;425:851–6.
11. Berman DM, Karhadkar SS, Maitra A, et al. Widespread requirement for Hedgehog ligand stimulation in growth of digestive tract tumours. Nature 2003;425:846–51.
12. Watkins DN, Berman DM, Burkholder SG, et al. Hedgehog signalling within airway epithelial progenitors and in small-cell lung cancer. Nature 2003;422:313–7.
13. Beachy PA, Karhadkar SS, Berman DM. Tissue repair and stem cell renewal in carcinogenesis. Nature 2004;432:324–31.
14. Garcea G, Dennison AR, Steward WP, et al. Role of inflammation in pancreatic carcinogenesis and the implications for future therapy. Pancreatology 2005;5:514–29.
15. Farrow B, Evers BM. Inflammation and the development of pancreatic cancer. Surg Oncol 2002;10:153–69.
16. Jura N, Archer H, Bar-Sagi D. Chronic pancreatitis, pancreatic adenocarcinoma, and the black box in-between. Cell Res 2005;15:72–7.
17. Luo JL, Maeda S, Hsu LC, et al. Inhibition of NF-κB in cancer cells converts inflammation-induced tumor growth mediated by TNFα to TRAIL-mediated tumor regression. Cancer Cell 2004;6:297–305.
18. Greten FR, Eckmann L, Greten TF, et al. IKKβ links inflammation and tumorigenesis in a mouse model of colitis-associated cancer. Cell 2004;118:285–96.
19. Friess H, Guo XZ, Nan BC, et al. Growth factors and cytokines in pancreatic carcinogenesis. Ann N Y Acad Sci 1999;880:110–21.
20. Apte RN, Voronov E. Interleukin-1—a major pleiotropic cytokine in tumor-host interactions. Semin Cancer Biol 2002;12:277–90.
21. Szlosarek PW, Balkwill FR. Tumour necrosis factor α: a potential target for the therapy of solid tumours. Lancet Oncol 2003;4:565–73.
22. Karin M, Greten FR. NF-κB: linking inflammation and immunity to cancer development and progression. Nat Rev Immunol 2005;5:749–59.
23. Wang W, Abbruzzese JL, Evans DB, et al. The nuclear factor-κB RelA transcription factor is constitutively activated in human pancreatic adenocarcinoma cells. Clin Cancer Res 1999;5:119–27.
24. Luo JL, Kamata H, Karin M. IKK/NF-κB signaling: balancing life and death—a new approach to cancer therapy. J Clin Invest 2005;115:2625–32.
25. Iwamura T, Katsuki T, Ide K. Establishment and characterization of a human pancreatic cancer cell line (SUIT-2) producing carcinoembryonic antigen and carbohydrate antigen 19-9. Jpn J Cancer Res 1987;78:54–62.
26. Kubo M, Nakamura M, Tasaki A, et al. Hedgehog signaling pathway is a new therapeutic target for patients with breast cancer. Cancer Res 2004;64:6071–4.
27. Fan L, Pepicelli CV, Dibble CC, et al. Hedgehog signaling promotes prostate xenograft tumor growth. Endocrinology 2004;145:3961–70.
28. Sasaki H, Nishizaki Y, Hui C, et al. Regulation of Gli2 and Gli3 activities by an amino-terminal repression domain: implication of Gli2 and Gli3 as primary mediators of Shh signaling. Development 1999;126:3915–24.
29. Sato S, Sugiyama M, Yamamoto M, et al. Toll/IL-1 receptor domain-containing adaptor inducing IFN-β (TRIF) associates with TNF receptor-associated factor 6 and TANK-binding kinase 1, and activates two distinct transcription factors, NF-κB and IFN-regulatory factor-3, in the Toll-like receptor signaling. J Immunol 2003;171:4304–10.

30. Yamanaka N, Morisaki T, Nakashima H, et al. Interleukin 1β enhances invasive ability of gastric carcinoma through nuclear factor-κB activation. Clin Cancer Res 2004;10:1853–9.
31. Nakahara C, Nakamura K, Yamanaka N, et al. Cyclosporin-A enhances docetaxel-induced apoptosis through inhibition of nuclear factor-κB activation in human gastric carcinoma cells. Clin Cancer Res 2003;9: 5409–16.
32. Feig BW, Lu X, Hunt KK, et al. Inhibition of the transcription factor nuclear factor-κB by adenoviral-mediated expression of IκBα M results in tumor cell death. Surgery 1999;126:399–405.
33. Arlt A, Vorndamm J, Muerkoster S, et al. Autocrine production of interleukin 1β confers constitutive nuclear factor κB activity and chemoresistance in pancreatic carcinoma cell lines. Cancer Res 2002;62: 910–6.
34. Kusano KF, Pola R, Murayama T, et al. Sonic hedgehog myocardial gene therapy: tissue repair through transient reconstitution of embryonic signaling. Nat Med 2005;11:1197–204.
35. Watkins DN, Peacock CD. Hedgehog signalling in foregut malignancy. Biochem Pharmacol 2004;68: 1055–60.
36. Ohta M, Tateishi K, Kanai F, et al. p53-Independent negative regulation of p21/cyclin-dependent kinase-interacting protein 1 by the sonic hedgehog-glioma-associated oncogene 1 pathway in gastric carcinoma cells. Cancer Res 2005;65:10822–9.
37. Pasca di Magliano M, Hebrok M. Hedgehog signalling in cancer formation and maintenance. Nat Rev Cancer 2003;3:903–11.
38. Farrow B, Sugiyama Y, Chen A, et al. Inflammatory mechanisms contributing to pancreatic cancer development. Ann Surg 2004;239:763–9; discussion 769–71.
39. Raetz CR, Whitfield C. Lipopolysaccharide endotoxins. Annu Rev Biochem 2002;71:635–700.

Quantitative Analysis of Human Telomerase Reverse Transcriptase in Pancreatic Cancer

Kenoki Ohuchida,[1] Kazuhiro Mizumoto,[1] Daisuke Yamada,[1] Hiroshi Yamaguchi,[2] Hiroyuki Konomi,[1] Eishi Nagai,[1] Koji Yamaguchi,[1] Masazumi Tsuneyoshi,[2] and Masao Tanaka[1]

Abstract Although telomerase activity is a promising diagnostic marker, clinical introduction of this marker for cancer diagnosis is still problematic due to the lack of means of evaluating sample quality. Human telomerase reverse transcriptase (hTERT), one of the subunits of telomerase, is also a promising diagnostic marker. In the present study, we did large-scale analysis of 88 pancreatic juice samples to determine the feasibility of quantitative analysis of hTERT mRNA for diagnosis of pancreatic cancer. We found significant differences in hTERT expression among carcinoma-derived, intraductal papillary mucinous neoplasm (IPMN)–derived, and chronic pancreatitis–derived juice samples. Results showed that quantitative analyses of hTERT mRNAs are more useful in discriminating carcinoma from IPMN than from chronic pancreatitis. When the specificity was set at 100%, the sensitivity for differentiation between carcinoma and IPMN was 43.5%, whereas the sensitivity of cytologic examination was 22.0%. There were significant differences in hTERT expression among carcinoma cells, IPMN cells, and normal ductal cells isolated from pancreatic tissues by microdissection. Lymphocytes and hyperplastic epithelial cells isolated from tissues with the histologic appearance of pancreatitis showed various expression levels of hTERT. Our results suggest that quantitative analysis of hTERT mRNA in pancreatic juice is advantageous over cytologic analysis for differentiation between carcinoma and IPMN but probably not for differentiation between carcinoma and chronic pancreatitis.

Pancreatic cancer is the fifth leading cause of cancer death and has the lowest patient survival rate of any solid cancer (1, 2). Despite improvements in diagnostic imaging, diagnosis before surgery remains difficult due to the inaccessibility of the pancreas and surrounding organs. The vast majority of patients with pancreatic cancer suffer from a poor clinical outcome.

Endoscopic retrograde cholangiopancreatography (ERCP) is currently used as a diagnostic tool to distinguish pancreatic cancer from nonmalignant disorders (3, 4). However, chronic pancreatitis is one of these nonmalignant pancreatic diseases, and its ERCP features are often similar to those of pancreatic cancer. Therefore, several diagnostic strategies, employing cytology, DNA mutation markers, or aberrant expression of cancer-specific mRNA in pancreatic juice, have been reported for differential diagnosis between pancreatic cancer and chronic pancreatitis (5–7). Although these modalities have provided some benefits for diagnosis of pancreatic cancer, they have not yet been used worldwide.

Cystic lesions of the pancreas are being detected with increasing frequency due to application of diagnostic imaging technologies, such as computed tomography and magnetic resonance. Therefore, ERCP is being used with increasing frequency to further evaluate the cystic lesions identified by imaging studies. Intraductal papillary mucinous neoplasm (IPMN) and mucinous cystic neoplasm are the representative cystic neoplasms of the pancreas. Notably, since its first description by Ohhashi et al. in 1982 (8), IPMN has become an increasingly recognized cystic tumor with unique histopathologic features, including intraductal papillary growth, mucin hypersecretion, and resultant dilation of the pancreatic duct. IPMN is often associated with pancreatic cancer (9), occurring either as a separate lesion or as carcinoma derived from the IPMN. However, ERCP and other conventional diagnostic imaging modalities are not useful in evaluating the malignant potential of IPMN. This suggests that a diagnostic strategy to discriminate IPMN associated with cancer from benign IPMN is needed.

Telomerase activity is a promising diagnostic marker for pancreatic cancer (10, 11). We and other investigators have reported that detection of telomerase activity in pancreatic juice is useful for the diagnosis of pancreatic cancer (12–14). However, clinical introduction of this marker for cancer diagnosis is still problematic due to the lack of means of

Authors' Affiliations: Departments of [1]Surgery and Oncology and [2]Anatomic Pathology, Graduate School of Medical Sciences, Kyushu University, Fukuoka, Japan

Received 8/23/05; revised 10/24/05; accepted 11/9/05.

Grant support: Ministry of Education, Culture, Sports, Science and Technology of Japan, the Japan Society for the promotion of Science for Young Scientists.

The costs of publication of this article were defrayed in part by the payment of page charges. This article must therefore be hereby marked *advertisement* in accordance with 18 U.S.C. Section 1734 solely to indicate this fact.

Requests for reprints: Kazuhiro Mizumoto, Department of Surgery and Oncology, Graduate School of Medical Sciences, Kyushu University, 3-1-1 Maidashi, Fukuoka 812-8582, Japan. Phone: 81-92-642-5440; Fax: 81-92-642-5458; E-mail: mizumoto@med.kyushu-u.ac.jp.

doi:10.1158/1078-0432.CCR-05-1821

evaluating sample quality and the difficulties of quantitative measurement. Human telomerase reverse transcriptase (hTERT) is one of the subunits of telomerase, and its mRNA has been reported as a promising diagnostic marker (15–18). We have reported accurate quantitative analysis of hTERT mRNA in pancreatic juice obtained during ERCP (19). However, we were unable to show the utility of hTERT analysis of pancreatic juice for diagnosis of pancreatic cancer possibly due to the small number of samples.

In the present study, we did a large-scale analysis of 88 samples of pancreatic juice and determined the feasibility of quantitative analysis of hTERT mRNA to differentiate pancreatic cancer from IPMN or chronic pancreatitis. hTERT mRNA levels were significantly greater in carcinoma-derived juice samples than in pancreatitis-derived or IPMN-derived samples. The preoperative diagnostic utility of quantitative analysis of hTERT in pancreatic juice was evaluated by means of receiver operating characteristic (ROC) curves (20). To support the results of the analyses with pancreatic juice, we used microdissection to isolate normal ducts, IPMN cells, and invasive ductal carcinomas (IDC) and examined the levels of hTERT expression in the cells. In addition, we isolated lymphocytes and hyperplastic epithelial cells from pancreatic tissues with the histologic appearance of pancreatitis and investigated their hTERT expression levels.

Materials and Methods

Pancreatic juice and pancreatic tissues. Pancreatic juice samples were collected from 88 patients who had undergone ERCP for suspected malignancy of the pancreas at Kyushu University Hospital (Fukuoka, Japan) from January 1, 2002 to December 31, 2004 as described previously (12, 21). We used pellets of cellular material from pancreatic juice for preparation of RNAs. The diagnosis of pancreatic ductal adenocarcinoma was confirmed by histologic examination of resected specimens when available (12 cases), but when the case was inoperable a clinical diagnosis was made based on imaging findings (11 cases). Pancreatitis or IPMN was diagnosed based on histologic examination of resected specimens or clinical findings at the time of the initial diagnosis and during a follow-up of at least 6 months that included conventional diagnostic imaging. Tissue samples were obtained at the time of surgery at Kyushu University Hospital. Thirteen IDC or 8 IPMN tissue samples were obtained from the primary tumor of each resected pancreas, and 18 nonneoplastic tissues (normal pancreas, 8 samples; pancreatitis, 10 samples) were taken from peripheral tissues away from the tumor in each patient. The tissue samples were removed as soon as possible after resection and divided into at least two bulk tissue samples. A part of each sample was embedded in OCT compound (Sakura, Tokyo, Japan) and snap-frozen for analysis by microdissection. The remainder was fixed in formalin, embedded in paraffin, and cut into 4-μm-thick sections for H&E staining. All tissues adjacent to the specimens were examined histologically, and the diagnosis was confirmed. Written informed consent was obtained from all patients, and the study was conducted according to the guidelines of the Helsinki declaration.

Quantitative analysis of hTERT mRNA levels by real-time PCR. Total RNA was extracted from cell pellets of pancreatic juice and cells isolated by microdissection techniques as described previously (22). We designed a real-time PCR protocol for the quantitative analysis of hTERT and β-actin mRNAs and did quantitative real-time PCR with a Quantitect SYBR Green RT-PCR kit (Qiagen, Tokyo, Japan) using a LightCycler Quick System 350S (Roche Diagnostics, Mannheim, Germany) as described previously (19). Briefly, the reaction mixture was first incubated at 50°C for 15 minutes to allow for reverse transcription. PCR was then initiated at 95°C for 10 minutes to activate modified Taq polymerase followed by a 45-cycle amplification (95°C for 15 seconds, 55°C for 20 seconds, and 72°C for 10 seconds) and 1 cycle (95°C for 0 second, 65°C for 15 seconds, and 0.1°C/s to 95°C) for melting analysis. Each sample was run twice. In addition, all samples showing >10% deviation in values were tested in a third run. The 10% deviation was calculated from concentrations after use of the calibration curve. mRNA expression of each sample was calculated from a standard curve constructed with the use of total RNA from the Capan-1 pancreatic cancer cell line. The range of threshold cycles observed was 20 to 35 cycles for hTERT and 15 to 30 cycles for β-actin primers. For relative quantification, the expression of hTERT mRNA was normalized to that of β-actin mRNA.

Microdissection-based quantitative analysis of mRNA. The frozen tissue samples were cut into 8-μm-thick sections. One section was stained with H&E for histologic examination. IDC cells, IPMN cells, normal pancreatic ductal epithelial cells, hyperplastic epithelial cells, and lymphocytes were isolated selectively by means of laser microdissection and a pressure catapulting system (Palm Microlaser Technologies, Bernried, Germany) in accordance with the manufacturer's protocols. After microdissection, total RNA was extracted from the selected cells and subjected to real-time PCR for quantitative measurement of hTERT mRNA.

Statistical analyses. Data were analyzed by Mann-Whitney *U* test because normal distributions were not obtained. Statistical significance was defined as $P < 0.05$, but because we did multiple comparisons on our real-time PCR data in the analyses of pancreatic juice samples we conservatively used Bonferroni correction; thus, the adjusted significance level was $P < 0.0167$ in the analyses of pancreatic juice. The optimal cutoff points for each marker for discriminating between pancreatic carcinoma and other benign diseases were sought by constructing ROCs, which were generated by calculating the sensitivities and specificities of each marker at several predetermined cutoff points (23).

Results

Quantitative analysis of hTERT mRNA expression in pancreatic juice. We measured hTERT mRNA expression levels in 88 pancreatic juice samples, including 23 from pancreatic carcinomas, 29 from IPMN, and 36 from chronic pancreatitis. Relative expression of hTERT was significantly greater in carcinoma samples than in chronic pancreatitis or IPMN samples after Bonferroni correction (Fig. 1; $P < 0.016$ for carcinoma versus chronic pancreatitis and $P < 0.0004$ for carcinoma versus IPMN). The difference in hTERT mRNA expression between IPMN and chronic pancreatitis samples was not significant after Bonferroni correction was applied (Fig. 1; $P = 0.0304$).

ROCs for hTERT mRNA expression are presented in Fig. 2. The sensitivity of each marker was determined at several specificity levels. The area under the ROC was 0.778 for carcinoma versus IPMN [95% confidence interval (95% CI), 0.636-0.884] and 0.629 for carcinoma versus chronic pancreatitis (95% CI, 0.479-0.762). In particular, a significant difference between the areas for carcinoma versus IPMN and carcinoma versus chronic pancreatitis was observed (difference between areas, 0.149; 95% CI, 0.005-0.293; $P = 0.042$). These data reveal that the discriminative ability for carcinoma versus IPMN is greater than that for carcinoma versus chronic pancreatitis.

In this study, cytologic class 4 or 5 (24) was considered positive for a diagnosis of malignancy. The cytologic sensitivity for diagnosis of pancreatic cancer was only 22.0% (95% CI, 14.7-29.3), which was similar to that cited in previous reports (12), although the specificity was 100%. The ROC analyses